Journal Pre-proof

How minor structural changes generate major consequences in photophysical properties of RE coordination compounds; resonance effect, LMCT state

Ewa Kasprzycka, Albano N. Carneiro Neto, Victor A. Trush, Lucjan Jerzykiewicz, Vladimir M. Amirkhanov, Oscar L. Malta, Janina Legendziewicz, Paula Gawryszewska

PII: S1002-0721(19)30962-7

DOI: https://doi.org/10.1016/j.jre.2020.02.001

Reference: JRE 702

To appear in: *Journal of Rare Earths*

Received Date: 1 December 2019

Revised Date: 3 February 2020

Accepted Date: 4 February 2020

Please cite this article as: Kasprzycka E, Carneiro Neto AN, Trush VA, Jerzykiewicz L, Amirkhanov VM, Malta OL, Legendziewicz J, Gawryszewska P, How minor structural changes generate major consequences in photophysical properties of RE coordination compounds; resonance effect, LMCT state, *Journal of Rare Earths*, https://doi.org/10.1016/j.jre.2020.02.001.

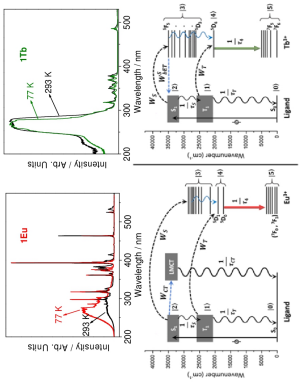
1Tb
77 K
293 K
Intensity / Arb. Units
Wavelength / nm
200
300
400
500
Ligand
Tb3+
1Eu
77 K
293 K
Intensity / Arb. Units
Wavelength / nm
Ligand
Eu3+

How minor structural changes generate major consequences in photophysical properties of RE coordination compounds; resonance effect, LMCT state.

EwaKasprzycka[a], Albano N. Carneiro Neto[b], Victor A. Trush[c], LucjanJerzykiewicz[d], Vladimir M. Amirkhanov[c], Oscar L. Malta[e], Janina Legendziewicz[d] and Paula Gawryszewska*[d]

[a]*University of Applied Sciences - FachhochschuleMünster, Department of Chemical Engineering, Stegerwaldstr. 39, Steinfurt, 48565, Germany*

[b]*Physics Department and CICECO-Aveiro Institute of Materials, University of Aveiro, 3810-193 Aveiro, Portugal*

[c]*Department of Chemistry, Taras Shevchenko National University of Kyiv, ul. Volodymyrska 64, Kyiv 01601, Ukraine*

[d]*Faculty of Chemistry, University of Wroclaw, 14 F. Joliot-Curie Street, 50–383 Wroclaw, Poland*

[e]*Departamento de Química Fundamental Universidade Federal de Pernambuco Cidade Universitária, Recife-PE, 50740–560, Brazil*

***Corresponding author, email:**paula.gawryszewska@chem.uni.wroc.pl

Keywords:lanthanide, phosphorylated sulfonamides, energy transfer, antenna effect, crystal structure, resonance effect

Abstract:

Lanthanide coordination compounds of the formula $Na[Ln(L)_4]$ (**1Ln**), where Ln = La^{3+}, Eu^{3+}, Gd^{3+}, Tb^{3+}, L = $[L]^-$ and HL = dimethyl(4-methylphenylsulfonyl)amidophosphate, were synthesized. Their structural and spectroscopic properties were discussed in detail based on X-ray diffraction measurements, IR spectroscopy, absorption and emission spectroscopy at 293 and 77 K and theoretical calculations of the intramolecular energy transfer (IET) rates. DFT calculations were used to investigate the **1Ln** electronic properties required to calculate

the transition rates. 30 and 22 pathways of intramolecular nonradiative energy transfer were examined in the case of **1Eu** and **1Tb**, respectively. It was shown that the main pathway for sensitization of the lanthanide emission is either the triplet (**1Eu**) or singlet (**1Tb**) transfer, occurring mainly through the exchange mechanism. The energy rates for energy transfer from S_1 and T_1 equal $W_S = 1.53 \times 10^5 s^{-1}$ (**1Eu**), $W_T = 5.14 \times 10^6 s^{-1}$ (**1Eu**) and $W_S = 4.09 \times 10^7 s^{-1}$ (**1Tb**), $W_T = 6.88 \times 10^5 s^{-1}$ (**1Tb**). The crucial role of the $^7F_5$ level in the energy transfer process of **1Tb** andthe participation of the LMCT state in the depopulation of the ligand singlet state of **1Eu** was demonstrated. The influence of the resonance effect on the splitting of the $^7F_1$ level in **1Eu** was analyzed. By comparing the properties of **1Ln** with the properties of **2Ln** coordination compounds, sharing the same ligand and crystallizing in the same crystallographic system (monoclinic), but with a different space group, it was demonstrated how slight structural changes can affect the photophysical properties of Ln compounds.

1. Introduction

Lanthanide compounds are intensively studied due to their interesting emission properties, such as: long micro- and milliseconds orders of emission lifetime; narrow emission bands, the location of which practically does not depend on the crystal field; high emission quantum yield; photostability. These features cause that lanthanide compounds are used as luminescent materials in biology and medical diagnostics, [1–3]in lighting and OLED devices, [4] in solar cells, [5-6]. However, Ln^{3+} emission requires sensitization due to the low values of the molar absorption coefficient.

One way to sensitize is to use an organic ligand as a sensitizer, which after the absorption process transfers the excitation energy via a nonradiative process to Ln^{3+} excited levels (antenna effect). [7] This allows the achieving of strong sensitized photoluminescence of lanthanide. In the context of the antenna effect, it is important to know the paths and mechanisms of energy transfer as well as the impact of structural modification on the sensitized emission of lanthanide. Knowledge of these issues is helpful in designing coordination compounds with specific luminescent properties. The aspects discussed in the paper raise the above-mentioned issues.

In this paper, we demonstrate how small structural differences resulting from the presence or absence of solvent molecules in the second coordination sphere determine the photophysical properties of **1Ln** and **2Ln**. The work also focuses on the analysis of ligand-to-metal energy transfer mechanisms with the participation of higher excited levels of

lanthanides as well as assuming the population of the $^7F_5$ and $^7F_1$ levels of Tb^{3+} and Eu^{3+}, respectively. An important element is also the correlation of structural and spectroscopic results for **1Eu** in the context of some restrictions on the use of Eu^{3+} as a structural probe for monomeric compounds with one Eu^{3+} crystallographic position. The presented results are a continuation of the research on Ln coordination compounds with N-phosphorylated amides [8–13] which were planned so as to eliminate from the chelate ring the atom groups of the C—H, N—H or C=O type responsible for high-energy vibrations.

2. Experimental Section

2.1 Synthesis

Unless otherwise specified herein, reagents were of analytical grade, obtained from commercial suppliers, and used without further purification. The preparation of dimethyl(4-methylphenylsulfonyl)amidophosphate (**HL**) (Figure 1) as well as its sodium salt (**1Na**) was carried out according to the procedure described previously. [8, 14]

Complexes of **1Ln** (Ln= Eu, Gd, Tb) were synthesized in the same manner as the Nd^{3+} complex.[15]Briefly, the hydrated nitrate (V) of corresponding lanthanide was dissolved in small amount of acetone and dehydrated by triethylorthoformate. Subsequently, the solution was treated with **NaL** in the 1:4 mole ratio in acetone. The resulting precipitate was separated by filtration. Clear filtrate was left for slow evaporation with mixture of acetone and propan-2-ol in ratio 3:1 at room temperature. The crystals that formed after a few days were suitable for X-ray investigations.

The synthesis of complexes **2Ln** (Ln= Eu, Gd, Tb) has previously been described in the literature.[8]The **2Ln** complexes were obtained by refluxing crystals of **1Ln** with acetonitrile for 2 hours. Slow evaporation in the mixture of acetonitrile and isopropanol in the ratio 1:1 resulted in crystalline solids proper to study by single crystal X-ray diffraction.

1Tb: yield 91%, IR(nujol): ν_{max} = 2923, 1462, 1377, 1254, 1176, 1033, 864, 750, 665, 562, 443, 341, 297, 152, 73, 57 cm^{-1}; IR(fluorinated oil): ν_{max} = 3006, 2956, 2853, 2328, 1600, 1498, 1456, 1397, 1385 cm^{-1}.

2Eu: yield 85%, IR(nujol): ν_{max} = 2916, 1464, 1377, 1252, 1173, 1051, 865, 745, 666, 562, 444, 333, 297, 155, 100, 73, 56 cm^{-1}; IR(fluorinated oil): ν_{max} = 3002, 2956, 2854, 2319, 1715, 1599, 1448, 1399, 1363 cm^{-1}.[8]

Figure 1.

2.2 Crystal structure determination

Diffraction data for **1Tb** and **1Eu** crystals were collected on an Agilent an Xcalibur four-circle diffractometer with Mo Kα radiation and a Ruby charge-coupled device detector. The collected diffraction data (1–2) were processed with the CrysAlis PRO program. [16] All structures were solved by direct methods using the SHELXS and refined by full-matrix least-squares on F^2 using the SHELXL programs. [17]Analytical absorption corrections were applied. In all structures the H atoms of aromatic rings were treated as riding atoms in geometrically idealized positions, with C—H = 0.095 nm and Uiso(H) = 1.2 Ueq(C) as well as H atoms of methyl groups were introduced in positions calculated from geometry, with C—H = 0.098 nm and Uiso(H) = 1.5 Ueq(C). Moreover, some atoms in the $-OCH_3$ substituent groups are disordered and were reined using a split model. The program used for molecular graphics is DIAMOND. [18]Crystallographic data for the structures reported in this paper have been deposited as supplementary publication nos. CCDC 1968705 (**1Eu**) and CCDC 1968744 (**1Tb**).These data can be obtained free of charge from The Cambridge Crystallographic Data Centre via www.ccdc.cam.ac.uk/data_request/cif.

2.3 Methods

Fourier transform infrared (FTIR) spectroscopy was performed using a Brücker IFS66/S FTIR spectrophotometer, in the range between 4000 and 50 cm^{-1} with a resolution of 1 cm^{-1}. An average of 8 scans was carried out for each sample. The samples were prepared using nujol and fluorinated oil emulsions (only in the near infrared range).

Reflectance measurements were performed using a Cary-Varian 500 spectrophotometer with barium sulfate as a reference at room temperature. Absorption spectra were recorded with a Cary 5000 Series UV/Vis-NIR Spectrophotometer. The spectra of samples as KBr pellets were measured at room temperature.

The fluorescence spectra were measured using a SpectraPro 750 emission line from Action Research Corporation. The excitation source was a 450 W Xe arc lamp coupled with an excitation monochromator using an 1800 L/mm grating blazed at 250 nm and an emission monochromator using 1200 L/mm grating blaze at 500 nm. A photomultiplier Hamamatsu R928 was used for detection. Samples were measured at room temperature using a solid sample holder on special 1.5 mm deep plexiglass plates. High-resolution uncorrected emission spectra were recorded using the same device at room and low temperature (77 K) by placing the sample in a quartz test tube in a quartz Dewar cooled by liquid nitrogen.

The corrected emission and excitation spectra of **1Eu** and **1Tb**were recorded using an FSL 920 Spectrometer from Edinburgh Instruments. A Xe arc lamp (450 W) was used as the excitation source and a red-sensitive photomultiplier (Hamamatsu R-928) as a detector. The luminescence decay curves of studied compounds were also registered with the same device using µF920H 60 W Xe flash lamp for phosphorescence (at 77K) and luminescence from excited levels of Eu^{3+} and Tb^{3+} (at 293 and 77K).

Emission quantum yield of europium and terbium complexes were determined in the same manner as described previously, [8]using the comparative method in which the sample under examination is compared to a standard with known quantum yield. Gd_2O_2S:3%Eu (GOS:Eu, q_{st} = 100%)and Gd_2O_2S:3%Tb (GOS:Tb, q_{st} = 100%)were used as emission standards and $BaSO_4$ as a reflectance standard(r = 91%).

2.4 Theoretical calculations

A DFT level of theory was employed to obtain the electronic properties like the composition of the excited triplet (T_1) and singlet (S_1) states of the ligand (*i*), the localization of molecular orbitals (LMOs) from the canonical ones (*ii*), and to obtain the overlap integrals (*iii*).

(i) TD-DFT was performed using the Gaussian 09 program [19]with the ωB97-XD functional [20] and aug-cc-pVTZ[21] basis set (for H, C, N, O, P, and S atoms).

(ii) LMOs of the ligands were obtained using the Pipek-Mezey method. [22] The GAMESS program [23] with the ωB97-XD functional [20]and aug-cc-pVTZ[21] basis set was used for this procedure.

(iii) The overlap integrals (ρ) involved in the Ln^{3+}–O (Ln = Eu or Tb) chemical bonds (first coordination sphere) were calculated with the ADF program [24] using the BP86 functional, [25, 26] STO-TZ2P basis set, [27] and the inclusion of ZORA scalar relativistic effects. [28–30]

2.5 Energy transfer rates

Energy transfer rates from S_1 and T_1 to Eu^{3+} and Tb^{3+} ions

Here it is important to emphasize that the CGS system of units is used. The intramolecular energy transfer rates (IET) from the ligands (S_1 and T_1) to the Ln^{3+} ion were calculated taking into account the dipole–dipole ($W_{\mathrm{d-d}}$), dipole–multipole ($W_{\mathrm{d-m}}$), and exchange (W_{ex}) mechanisms, [31–34] according to Eqs. (1)–(3):

$$W_{\mathrm{d-d}} = \frac{S_{\mathrm{L}}(1-\sigma_1)^2}{(2J+1)G}\frac{4\pi}{\hbar}\frac{e^2}{R_{\mathrm{L}}^6}\sum_{\lambda}\Omega_K^{\mathrm{FED}}\langle\psi' J'\|U^{(K)}\|\psi J\rangle^2 F \quad (1)$$

$$W_{\mathrm{d-m}} = \frac{S_{\mathrm{L}}}{(2J+1)G}\frac{2\pi e^2}{\hbar}\sum_{K}(K+1)\frac{\langle r^K\rangle^2}{(R_{\mathrm{L}}^{K+2})^2}\langle f\|C^{(K)}\|f\rangle^2(1-\sigma_K)^2\langle\psi' J'\|U^{(K)}\|\psi J\rangle^2 F \quad (2)$$

$$W_{\mathrm{ex}} = \frac{(1-\sigma_0)^2}{(2J+1)G}\frac{8\pi}{\hbar}\frac{e^2}{R_{\mathrm{L}}^4}\langle\psi' J'\|S\|\psi J\rangle^2\sum_{m}\left|\left\langle\phi\left|\sum_j\mu_{\mathrm{z}}(j)s_m(j)\right|\phi^*\right\rangle\right|^2 F \quad (3)$$

whereΩ_K^{FED} (in Eq. (1)) are the intensity parameters assigned exclusively to the forced electric dipole mechanism (original Judd-Ofelt theory [35, 36]) and, in the present work, they were calculated using the Simple Overlap Model and the average energy denominator method [37, 38] as expressed by Eq. (S2). $\langle \|U^{(K)}\| \rangle^2$ are squared reduced matrix elements and their values are tabulated in Ref. 39.

In Eqs. (1) and (2), S_{L} is the dipole strength of the ligand transition involved in the IET process, $\langle r^K\rangle$ are $4f$ radial integrals, G is the degeneracy of the ligand donor state, $\langle \|C^{(K)}\| \rangle$ is a monoelectronic reduced matrix element of the Racah's tensor operators $\boldsymbol{C}^{(K)}$, and $(1-\sigma_K)$ are shielding factors. [34]

In Eq. (3), $(1-\sigma_0)$ can be estimated using the relationship $(1-\sigma_0) = \rho(R_{\min}/R_{\mathrm{L}})^{3.5}$, where $R_{\min}$ is the shortest Ln–O distance. This formulation has been discussed in detail in Ref.40. S_m is the spin operator in the ligand, μ_{z} is the dipole operator (its$z$-component), and $\langle\psi' J'\|S\|\psi J\rangle$ is the reduced matrix elements of the lanthanide ion spin operator, which were calculated (Supporting Information) using free-ion wavefunctions in the intermediate coupling scheme (angular momentum operators are used in units of Planck's constant over 2π). [41]

F in Eqs. (1)–(3) is the spectral overlap integral that expresses the energy mismatch conditions between donor and acceptor energy levels. [40, 42]

$$F = \frac{1}{\hbar\gamma_L}\sqrt{\frac{\ln(2)}{\pi}}e^{-\left(\frac{\Delta}{\hbar\gamma_L}\right)^2\ln(2)} \quad (4)$$

Where $\hbar\gamma_{\mathrm{L}}$ corresponds to the donor's (ligand) bandwidths at half-height (in erg units). $\Delta$is the energy difference between the barycenter of the donor state (D) and the lanthanide acceptor state, $\Delta = E_{\mathrm{D}} - E_{\mathrm{Ln}}$.There are four ligands coordinated with very close triplet states

and very close singlet states that redistribute energy between them extremely fast. So that, this fact is taken into account upon evaluation of the band half-widths entering in calculation of the energy mismatch factor F.

The forward energy transfer rates were calculated by the sum over Eqs. (1), (2) and (3) ($W = W_{\mathrm{d-d}} + \mathrm{W}_{\mathrm{d-m}} + W_{\mathrm{ex}}$) for each IET pathway under the following assumptions:

1) In the case of the Eu^{3+} ion, the thermal populations of the $^7F_0$ (0.64) and the $^7F_1$ (0.33), at 300 K, were taken into account. In the case of the IET pathway involving the $^7F_0 \rightarrow {}^5D_0$ transition, the *J*-mixing between the $^7F_0$ and $^7F_2$ levels (of the order of 5%) was considered.

2) In the case of the Tb^{3+} ion, once the first excited state, $^7F_5$, is curiously known to have an abnormally long decay lifetime (from 2.8 to 22 ms) [43–45] it plays a very important role in the IET kinetics, and consequently, in the emission quantum yield.

3) In both cases, when Δ is negative (the ligand donor state barycenter lies below the lanthanide acceptor level), the IET rates were multiplied by the barrier factor $e^{-\left(\frac{|\Delta|}{k_B T}\right)}$, where k_{B} is Boltzmann's constant and T is the temperature.

Energy transfer rates involving the LMCT state

According to the theoretical approach in Ref.46, the energy transfer between ligand and LMCT states is given by:

$$W_{\mathrm{CT}} = \frac{2\pi}{\hbar}\frac{e^4}{(R_{\mathrm{L}})^2}\langle 4f|\pi^*\rangle^2\langle\phi_0|\pi\rangle^2 F \qquad (5)$$

Where R_L is the distance from the Eu^{3+} ion to the electronic barycenter of the LMCT, which is expected to be shorter than the R_{L} value for IET rates in the previous cases (from S_1 and T_1 to Ln^{3+} states). $\langle 4f|\pi^*\rangle$ can be estimated using the same relationship as described to obtain $(1-\sigma_0)(\langle 4f|\pi^*\rangle = \rho(R_{\mathrm{min}}/R_{\mathrm{L}})^{3.5})$. $\langle\phi_0|\pi\rangle$ is the intramolecular overlap integral. Since, in this case, the bandwidths at half-height (γ_{CT} and γ_{L}) are of the same order of magnitude, the energy mismatch factor is given by [40, 46]:

$$F = \frac{\ln(2)}{\sqrt{\pi}} \frac{1}{\hbar^2 \gamma_L \gamma_{CT}} \left\{ \left[\left(\frac{1}{\hbar\gamma_{CT}} \right)^2 + \left(\frac{1}{\hbar\gamma_L} \right)^2 \right] \ln(2) \right\}^{-\frac{1}{2}}$$
$$\times \exp\left[\frac{1}{4} \frac{\left(\frac{2\Delta}{(\hbar\gamma_L)^2} \ln 2 \right)^2}{\left[\left(\frac{1}{\hbar\gamma_{CT}} \right)^2 + \left(\frac{1}{\hbar\gamma_L} \right)^2 \right] \ln 2} - \left(\frac{\Delta}{\hbar\gamma_L} \right)^2 \ln(2) \right] \quad (6)$$

Where the quantities γ_{CT} and γ_L are the bandwidths at half-height of the LMCT and the ligand states. Eq. (6) has the same meaning as Eq. (4) which is a simplified form of Eq. (6) when one of the bandwidths at half-height is much larger than the other one, As in the case of intramolecular energy transfer ligand-lanthanide ion ($\gamma_L \gg \gamma_{Ln}$). The quantity Δ is also the energy difference, but in this case, between the barycenter of the donor state (S_1) and the LMCT.

Concerning Eq. (5), we estimate (in *ad-hoc* mode) $R_L = 0.48$ nm and $\langle \phi_0 | \pi \rangle = 0.05$.

3. Results and discussion

3.1 X-ray analysis

1Ln coordination compounds (where Ln = La^{3+}, Eu^{3+}, Gd^{3+}, Tb^{3+}) crystallize in a monoclinic system in the $P2_1/c$ group and are isostructural. The crystallographic data for **1Eu** and **1Tb** are listed in Table S1. The coordination in **1Ln** is of the same kind as in other lanthanide coordination compounds with N-phosphorylated sulfonamides. [8–15, 47–49]The first coordination sphere consists of four bidentate deprotonatedligands(L^-), each of which is coordinated by two oxygen atoms of the sulfonyl and phosphoryl groups. The created anionic units $[LnL_4]^-$ are connected in a one-dimensional polymeric network with sodium ions. Figure 2 shows the **1Eu** crystal structure (CN = 8), crystal packing along the *c*-axis and a coordination polyhedron of the Eu^{3+} ion. Coordination polyhedrons of the metal ions in **1Eu** and **1Tb** were analyzed based on the SHAPE program, designed by Llunell et al. [50]Continous Shape Measures (CShMs) of the coordination geometry for the Ln^{3+} ions in **1Eu**, **1Tb**, **2Eu**, **2Tb** and point groupsare summarized in Table 1. **1Ln** and **2Ln** contain in their structure the same ligands which are also coordinated in the same manner by the metal ions. Despite such strong similarities, these compounds exhibit significantly different spectroscopic properties. This was the motivation for careful analysis of the structural properties of **1Ln** and comparison with crystallographic data of **2Ln** published in ref. 8. It should be emphasized that in both compound types the metal ion occupies a single crystallographic position with low point symmetry. Basing on the data from Table 1, the coordination polyhedrons in

1Lncanbedescribedas a distortedsquareantiprism, while the **2Ln** as a distorted triangulardodecahedron.

Table 1.

Ln–O bond lengths of **1Eu**, **1Tb**, **2Eu** and **2Tb** are listed in Table S2. Ln–O(P) bond lengths in **1Ln** and **2Ln** are comparable. On the other hand, all of the Ln–O(S) bond lengths are shorter in the case of **1Ln** in comparison with **2Ln**. Their average values are 2.445 (2) and 0.21.415 (3) nm in **1Eu** and **1Tb**, while they are equal to 0.2487 (2) and 0.2473 (2) nm in **2Eu** and **2Tb**. The angle values in the **1Ln** and **2Ln** chelate rings are comparable, and their average values are listed in Table S3. The Ln–Ln and Ln–Na distances in the chain are shorter in **1Ln** in comparison with **2Ln** by about 0.03 and 0.008 nm, respectively. Sodium ions have a coordination number of 6 in both types of compounds. They connect the anionic units $[LnL_4]^-$ via two oxygen atoms and one nitrogen atom of each unit.

Weak intramolecular C—H···π interactions (–OCH_3 group with the 4-methylphenyl ring) are present in **1Ln** and **2Ln**. The hydrogen atom of the –OCH_3 group is directed towards the center of the 4-methylphenyl ring of the same ligand and the distance between the aforementioned hydrogen atom and the center of the aromatic ring equals about 0.3 nm (see Table S4and Figure S1). There are no hydrogen bonds or intermolecular interactions in neither **1Ln** nor **2Ln**. The C—H···π interaction constitutes one of the important factors in controlling the crystal packing of the **1Ln** and **2Ln** molecules. An additional factor responsible for the packing in the **2Ln** molecule is the presence of disordered solvent molecules (acetonitrile) in the outer coordination sphere. In turn, in the **1Ln**structure, there is a disorder of the two –OCH_3groupsoftheligandsandofoneoxygenatomofthephosphorylgroup.

Figure 2.

3.2 Spectroscopic Analysis

3.2.1 IR Spectroscopy

Due to a large number of chemical bonds and the fact that most of the FTIR bands of the title compounds are located in the fingerprint region, the FTIR spectra are difficult to interpret, although it is still possible to observe some general common features between them. The FTIR spectra of lanthanide complexes **1Ln** and **2Ln** were recorded in the range 4000–50 cm^{-1}. Fig.3 and Fig.S2 show the **1Tb** and **2Eu** spectra as an example. It is noted that both

spectra are almost identical without noticeable shifts of band positions characteristic for the O=S=O and P=O groups, which occur at 1254 and 1177 cm^{-1} for **1Tb** and 1252 and 1173 cm^{-1} for **2Eu**. This phenomenon can be attributed to the fact that the complexes are almost identical and exhibit the same type of coordination. This was confirmed by comparison of the far infrared regions of the spectra (Figure S2), where the vibration bands of O–Ln–O fragment related to the chelate ring formed by the coordination is located.

Moreover, in contrast to the free ligand, in the FTIR spectra of both compounds, the absence of stretching vibrations of N–H group between 2850 and 2430 cm^{-1} can be observed. This confirms the complete deprotonation of nitrogen atoms in the complexes. Additionally, the lack of characteristic O–H stretching vibrations in the 3550–3200 cm^{-1} range indicates the absence of water molecules in the structure, which proves the purity of obtained complexes and is in good agreement with the crystallographic data. We would like to emphasize that the analysis of vibration bands in the range of 4000–1300 cm^{-1} was based on the spectra measured in fluorinated oil to eliminate the nujol bands.

Figure 3

3.2.2 Electronic state of the ligand

The **1Gd** and **1Tb** profiles of diffuse reflectance spectra recorded in the UV range are identical and the bands correspond to the $\pi^* \leftarrow \pi$ ligand absorption transitions. In contrast, the **1Eu** band is clearly broadened in the energy range 280–325 nm, which is shown in Figure 4. This widening indicates the contribution of the LMCT transition in the UV absorption region of **1Eu**. A comparison of the diffuse reflectance or absorption (tablets with KBr) spectra of the isostructural compounds of Eu^{3+} and Gd^{3+} or Eu^{3+} and La^{3+} (Y^{3+}) is a typical procedure for determining the contribution of LMCT transition in the absorption spectrum of the Eu^{3+} ion. [40]

Figure 4

For the experimental determination of the ligand triplet and singlet energy, the phosphorescence and fluorescence spectra of the ligand were measured for **1Na**, **1La** and **1Gd** at 77 and 293 K. The barycenter of the ligand triplet and singlet states of **1Ln** was determined as 23000 and 33000 cm^{-1} . The **1Gd** and **1La** phosphorescence spectra are shown in Figure 5 while the fluorescence spectra in Figure S3. The phosphorescence appears only at 77 K as a wide band in the range of about 370 to 550 nm for **1Na**, **1La**, and **1Gd**. No phosphorescence is observed in **1Eu** and **1Tb** emission spectra at low-temperature, which

indicates the appearance of additional channels of depopulation on the T_1 ligand state as compared to the **1Gd** one. The phosphorescence and fluorescence excitation spectra are almost identical and are presented in Figure 6.

The fluorescence of the ligand for**1Na**, **1La**, **1Tb** and **1Eu** is shown in Figure S3. In contrast to the ligand phosphorescence (**1Na**, **1La**, **1Gd**), the **1Ln** band undergoes widening by about 40 nm towards lower energies and a shift of the maximum by about 10 nm in comparison with **1Na**. From quantitative measurements of fluorescence intensity, it can be seen that the **1Eu** one is very weak in comparison with **1Tb**. As will be demonstrated in the latter part of this work, **1Eu** is characterized by much lower overall emission quantum yield in comparison with **1Tb**, which suggests that the opposite situation could be expected. Such low value of fluorescence intensity of **1Eu** implies the existence of an additional depopulation channel of the S_1 ligand state. Based on experimental data and theoretical calculations, the contribution of the charge transfer state (LMCT) to the depopulation of the S_1 ligand state was examined and the mechanism is discussed in paragraphs 3.2.3.2 and 3.3.

Figure 5.

Figure 6.

3.2.3 Photophysical properties of coordination compounds

3.2.3.1 Emission spectra – resonance effect

The **1Eu** and **1Tb** coordination compounds exhibit typical $^5D_0$ and $^5D_4$ emission at 300 and 77 K under excitation of either the lanthanide ion or the ligand. The emission spectra are presented in Figures S4 and S5. **1Tb** emission spectra are dominated by the $^5D_4 \rightarrow {}^7F_5$ transition band, while the **1Eu** emission spectra are dominated by the $^5D_0 \rightarrow {}^7F_2$ transition. The $^5D_0 \rightarrow {}^7F_0$ transition is present in **1Eu** emission spectra, proving that the Eu^{3+} ion is characterized by low point symmetry in the structure. The half-width of the $^5D_0 \rightarrow {}^7F_0$ band equals 9.8 cm^{-1} at 300 K and remains unchanged with the decrease of the temperature. The half-width value and the fact that it does not change after lowering the temperature are both caused by the disorder of the phosphoryl oxygen atomandofthetwo—OCH_3groupsoftheligands, which is demonstrated in Figure S6. When moving from a temperature of 300 to 77 K, a redshift of the $^5D_0 \rightarrow {}^7F_0$ band equals to 11.3 cm^{-1} is observed. The redshift of the $^5D_0 \rightarrow {}^7F_0$ band in the order of 10 cm^{-1} is known to take place in all Ln coordination compounds with N-phosphorylated sulfonamides. At 77 K, the $^5D_0 \rightarrow {}^7F_0$ band of

1Eu is characterized by a single symmetrical component, implying that the Eu^{3+} ion occupies one equivalent crystallographic position in the structure. This observation is also consistent with the crystallographic results. However, the number of components of the $^5D_0 \rightarrow {}^7F_1$ transition raises doubts. At 77 K, double number of electron components is observed in the form of zero-phonon line splitting or clearly visible bends present in the other electron lines. The number of Stark components of the $^5D_0 \rightarrow {}^7F_1$ transition is used to assess the number of crystallographic positions occupied by the Eu^{3+} ion in the crystal structure.[51] However, in the case of the $^5D_0 \rightarrow {}^7F_2$ and $^5D_0 \rightarrow {}^7F_4$ transitions, no more than $2J + 1$ electronic components are observed, which is shown in Figure 7. In the same figure, the emission transitions on **2Eu** are also seen, but they will be referred to in the latter part of this work.

Figure 7.

Due to the apparent inconsistency in the spectroscopic results for **1Eu**, measurements of emission and excitation spectra at 300 and 77 K were repeated for a single crystal, whose structure was confirmed by crystallography before the spectroscopic measurements. The measurement of the emission of such a small single crystal was possible due to the very large intrinsic emission quantum yield of **1Eu**. The obtained spectroscopic results were identical to the ones acquired in the case of several larger single crystals. The observed effect can be explained by the phenomenon of resonance effect. For achieving a confirmation on this, an analysis of the vibrational components was required. It should be emphasized that the purpose of this work was not to make a full analysis of the vibrational components, but to examine the vibrational coupling for the purpose of explaining the resonant effect.

In Figures S7 and S8 the vibrational components in the transition area of $^5D_0 \rightarrow {}^7F_0$, $^5D_0 \rightarrow {}^7F_2$ and $^5D_0 \leftarrow {}^7F_0$, $^5D_2 \leftarrow {}^7F_0$ are presented. The vibrational components extracted from the emission and excitation spectra are designated ν_n. Frequencies visible as vibrational components in the emission and excitation spectra are marked with an asterisk (*) in the FTIR spectra (see Figures3 and S2). The locations and frequencies of the vibrational components related to the vibrations in the IR spectrum are summarized in Table 2. The vibrational components correspond to the vibrations in the ligand (ν(PO),δ(OPO), ν(SO)) and vibrations in the chelate ring (ν(PO), ν(SN), ν(LnO),δ(OLnO) and γ(OLnO)) in **1Eu.** The crystal-field levels of the $^7F_1$ multiplet of the **1Eu** lie within the energy region of ν(Ln–O), their possible interactions result in "non-Born-Oppenheimer" states being the terminal states in the $^5D_0 \rightarrow {}^7F_1$

emission process. The mechanism of this phenomenon, in which a vibroniclevel is in resonance or near resonance with an electronic level was discussed by Malta.[52] Malta concluded that as a result of such resonance, the electronic line splitting occurs. Depending on the strength of the vibronic coupling and the degree of resonance, the resulting two lines may exhibit similar intensities. In the case of **1Eu** (see Figure 7), the splitting of the zero-phonon line of the $^5D_0 \rightarrow {}^7F_1$ transition (splitting value = 12.4 cm^{-1}) is observed as two components with almost identical intensities. The remaining two Stark components have clear bends and the use of the Lorentz distribution yields the following energy values: 16896.8 and 16879.4 cm^{-1}, 16790.9 and 16765.6 cm^{-1}. The resonance effect was also observed by the other authors in Ln coordination compounds with organic ligands [53–55]and inorganic ones as well. [56, 57] In the **1Eu** excitation spectrum, the resonance effect was not observed and the number of Stark components of the $^5D_1 \leftarrow {}^7F_0$ transition in 77 K is $2J + 1$ (see Figure S9). The half-width of the zero-phonon line (maximum at 19027 cm^{-1}) is 10 cm^{-1}. Due to equipment limitations, measurements of excitation spectra were not available at a higher resolution.

Table 2.

The analyzed example of **1Eu** demonstrates some restrictions on the usability of Eu^{3+} as a structural probe in compounds in which either the Eu^{3+} ion is well isolated by ligand molecules or the ones in which there is no Eu–Eu type energy transfer.

The resonance effect was not observed in the case of **2Eu**, even though the structural differences between **1Eu** and **2Eu** (see the crystallographic part of the paper) are seemingly minor. When comparing the $^5D_0$ emission in **1Eu** and **2Eu**, it turns out that the crystal field splitting values of the ^7F_J multiplet levels are much smaller in the case of **2Eu**. The splitting values of those levels in **2Eu** and **1Eu** equal 75 ($^7F_1$), 43 ($^7F_2$), 183 cm^{-1} ($^7F_4$) and 223 ($^7F_1$), 111 ($^7F_2$), 223 cm^{-1} ($^7F_4$), respectively (see Figure 7). The much smaller value of the ^7F_J levels splitting in **2Eu** is due to the fact that the point symmetry of the Eu^{3+} ion in **2Eu** is closer to the distorted dodecahedron and it mimics the spherical arrangement of donor atoms around the metal ion. In turn, the point symmetry of the Eu^{3+} ion in **1Eu** corresponds to a distorted squareantiprism (see Table 1).

It was also shown that **1Eu** can be obtained directly from **2Eu** by storing the crystal in air and evaporating the solvent from the second coordination sphere. This was confirmed by a simple experiment consisting of periodic measurements of emission of the (formerly structurally confirmed) **2Eu** stored in air ambiance. After several days, the measured

spectroscopic and structural properties started to correspond to **1Eu** what is shown in Figure S10. The single crystal did neither cloud nor fall apart.

3.2.3.2 Excitation spectra

Figures 7 and 8 present the **1Tb** and **1Eu** excitation spectra acquired at 77 and 293 K. The **1Tb** spectra are dominated by the ligand band in the range of 210–310 nm, which indicates good efficiency in sensitizing the Tb^{3+} emission. On the other hand, Eu^{3+} emission is not effectively sensitized by the ligand at neither 293 nor 77 K. Although the increase in ligand band intensity is observed at 77 K, the excitation spectrum is still dominated by the intra-configurational $4f^* \leftarrow 4f$ transitions. The impact of slight structural changes between **1Ln** and **2Ln** on the excitation spectra is illustrated in Figure 10. It turned out that the ligand band undergoes a shift and it is positioned in the 210–310 nm in the case of **1Ln**, while it is found within 240–333 nm in the case of **2Ln**.

Figure 8.

Figure 9.

Figure 10.

Analysis of the absorption spectra of **1Tb** and **2Tb** (see Figure S11) shows that the changes in the excitation spectra correlate with the change of the absorption band range. The edge of the **1Tb** absorption band lies at higher energy (about 300 nm) in comparison with the **2Tb** absorption band (about 330 nm). The presence of disordered solvent molecules in the second **2Ln** coordination sphere is considered responsible for the broadening of the absorption band of **2Tb** in relation to the one of **1Tb**. Furthermore, it is also possible that the presence of weak non-covalent interactions in the structure may contribute to the effect. However, due to the disorder of the solvent molecules, it is impossible to unambiguously discuss the non-covalent interactions and their participation basing solely on X-ray measurements. On the other hand, the occurrence of the surface quenching phenomenon causes a situation in which the maximum of the ligand band in the excitation spectrum does not correspond to the energy at the maximum of the band in the absorption spectrum, instead it falls only within the tail range of the absorption band. [58, 59] Surface quenching can be considered as a kind of internal filter effect, relying on the fact that electromagnetic radiation

from the high absorption range is strongly absorbed by the surface and as such does not reach the deeper layers of the sample. Less absorbed radiation stimulates both the outer and inner layers of the sample to emit and as a result, greater emission intensity is observed in this range of excitation radiation. The phenomenon of surface quenching causes that the shift of the absorption band edge by 30 nm can be easily noticed in the excitation spectrum. Differences in the photophysical properties of **1Ln** and **2Ln** compounds due to small structural changes also manifest themselves in the values of the overall emission quantum yield (Q_{Ln}^{L}) as well as in the temperature dependences of the sensitized Eu^{3+} emission efficiency.

Table 3 lists the values of intrinsic ($Q_{\mathrm{Ln}}^{\mathrm{Ln}}$) and overall emission quantum yield, efficiency of sensitization (η) and decay times established for **1Eu**, **1Tb**, **2Eu** and **2Tb**. The $Q_{\mathrm{Ln}}^{\mathrm{L}}$ is higher in the case of **1Tb** (58%) than the one of **2Tb** (36%). As the first coordination sphere is nearly identical in both cases, this result can be considered surprising. However, the increase in sensitized emission intensity between **1Tb** and **2Tb** is visually noticeable, in the same manner as the decrease in sensitized emission intensity is observed between **1Eu** and **2Eu**. The increase of $Q_{\mathrm{Ln}}^{\mathrm{L}}$ in the case of **1Tb** is tied to the shorter lengths of all of the Tb–O bonds (O of the sulfonyl group), which are on average 0.0058 nm shorter than in **2Tb**. Another important factor is the population of long-lived $^{7}F_{5}$ level of Tb^{3+} in **1Tb**,as demonstrated by the theoretical calculations of non-radiative rates and the overall emission quantum yield (see paragraph 3.3). Such calculations also prove to be very useful to investigate the impact of the LMCT (ligand-to-metal charge transfer) state on the reduction of the efficiency of sensitized emission in **1Eu** and **2Eu**. The location of the LMCT state for **1Eu** was estimated by comparing the diffuse reflectance spectra profiles of **1Eu** and **1Gd** (Figure 4).

It is well known [40] that the LMCT state can be an important quenching channel for the excited states of both ligand and Eu^{3+}. Depending on the energy of the LMCT state and the value of its parabola offset relative to the ligand and Eu^{3+} levels, non-radiative ligand → LMCT or Eu^{3+} → LMCT energy transfer may occur. The LMCT state can depopulate the S_1 or T_1 state of the ligand, reducing the sensitization efficiency of Eu^{3+} emission and thus yielding a lower $Q_{\mathrm{Ln}}^{\mathrm{L}}$. The magnitude of the LMCT effect on the value of $Q_{\mathrm{Ln}}^{\mathrm{L}}$ depends on the value of the overlap integral between the wavefunctions of the LMCT and π states. The energy of the LMCT state is strongly temperature dependent, and as such the influence of LMCT on sensitized Eu^{3+} emission should be temperature dependent as well. This is observed in the case of **1Eu** (see Figure 9), in contrast to **2Eu**. [8]Lifetime of the **1Eu** $^{5}D_{0}$ emission is

independent of both temperature and excitation wavelength. This behavior reflects the absence of thermally activated non-radiative processes, either vibrational or electronic in nature, including the $^5D_0$ emitting levels. The decayprofilesof**1Eu** ($^5D_0$) and**1Tb** ($^5D_4$) emissionaremonoexponential. The values of **1Ln** and **2Ln** emission lifetimes are summarized in Table 3. In order to describe the effects of the LMCT states on the Ln^{3+} emission, models for the description of the energy transfer processes Ln^{3+} → LMCT and ligand → LMCT have been developed. [60] This model is used to prove the participation of LMCT in the energy transfer process in **1Eu**.

Table 3.

3.3 Theoretical calculations

3.3.1 Intramolecular energy transfer rates.

To rationalize the experimental results and to propose the ligand-to-metal energy transfer mechanism intramolecular energy transfer (IET) rates were calculated for **1Eu** and **1Tb**. In the calculations for **1Eu**, the energy transfer between the ligand and the LMCT state was taken into account. As discussed earlier, the diffuse reflectance spectrum for the **1Eu** complex, shown in Figure 4, a LMCT band around 33300 cm^{-1} is clearly identified, in contrast to the case of **2Eu**[8] where this band is possibly hidden and mixed with the S_1 state.

The donors–acceptor distances (R_L) are crucial information for the energy transfer evaluation, and, in this work, they were obtained from TD-DFT calculations (item *(i)* in the experimental section) by isolating the ligands from the crystallographic structure. The donors (Singlet and Triplet states) centers are localized at the aromatic rings, as depicted inFigure 11. Therefore, we can assume that R_L is an average between the distances from the middle of the aromatic rings to the Ln^{3+} ion, leading to a value of 5.8 Å. This is represented in Figure S12.

Figure 11.

On the other hand, the distance from the Eu^{3+} ion to the electronic barycenter of the LMCT state was estimated as 0.48 nm (see experimental section).

We have analyzed a total of 30 and 22 pathways for Eu^{3+} and Tb^{3+}, respectively. All pathways were chosen based on selection rules and theΔ values. [40] The necessary quantities

for the evaluations of the IET rates are displayed in Tables S5and S6 and the results (IET for each pathway) are shown in Tables S7and S8.

According to Tables S7 andS8, it can be noticed that, for **1Eu**, the dominant pathways come from the T_1 state, while for the case of **1Tb** the most relevant pathways come via S_1. The total energy transfer from S_1 and T_1 are equal to $W_S = 1.53 \times 10^5 s^{-1}$ (**1Eu**), $W_T = 5.14 \times 10^6 s^{-1}$(**1Eu**) and $W_S = 4.09 \times 10^7 s^{-1}$ (**1Tb**), $W_T = 6.88 \times 10^5 s^{-1}$(**1Tb**). This is a noteworthy aspect in comparison with the results obtained for **2Eu**. [8] In our interpretation, this is due to the action of a LMCT state close to the ligand singlet state. The LMCT state has usually a very short decay lifetime (of the order or shorter than nanoseconds), and in the present case, it would quite suppress the action of the singlet S_1 in feeding the state T_1. It is important to notice that the LMCT state is about 300 cm^{-1} above the ligand S_1 state, and it is energetically much far apart (~10000 cm^{-1}) from the ligand state T_1. The energy transfer from the S_1 to the LMCT state is equal to $W_{CT} = 4.82 \times 10^8 s^{-1}$.

3.3.2 The role of the Tb^{3+} $^7F_5$ level in IET processes

Due to a large decay lifetime of the $^7F_5$ level (from 2.8 to 22 ms) [43–45]this level population, in the steady-state regime, has important participation as acceptor state, as it can be clearly seen in the $^7F_5 \rightarrow {}^5D_4$, pathways 9, 10 and 17 in Table S8. The abnormal long lifetime of this level is still not understandable, once one could easily raise the point on the multiphonon decay to the $^7F_6$ ground state. However, this is an experimental fact, [44, 45] and taking this into account may explain much of the emission quantum yield properties of Tb^{3+} compounds.

3.3.3 Emission quantum yields

From the appropriate rate equations in the steady-state regime (Supporting Information), the level normalized populations (N_i) and subsequently the emission quantum yields Q_{Ln}^{L} were calculated based on the energy levels diagrams in Figure 12.

Figure 12.

Q_{Ln}^{L} is then given by (Supporting Information):

$$Q_{\mathrm{Ln}}^{\mathrm{L}} \cong \frac{A_{\mathrm{rad}} N_4}{\phi} \tag{7}$$

We assume that the ground states normalized populations are very little depleted and, therefore, they are taken approximately equal to 1. In this procedure, it is not difficult to see that the pumping rate ϕ cancels and $Q_{\mathrm{Ln}}^{\mathrm{L}}$ turns out to be independent of it. However, this does not mean that $Q_{\mathrm{Ln}}^{\mathrm{L}}$ could not eventually depend on the pumping excitation energy. In Eq. (7), the radiative rate A_{rad} is the sum of all radiative channels from the emitting lanthanide level. The results are summarized in Table 4.

Table 4.

It is known that the S_1 and T_1 lifetimes drop down dramatically to the ranges of nanosecond and microsecond, respectively, at room temperature. We can obtain a perfect agreement between theory and experiment for both complexes, as shown in Table 4, taking the values of τ_S = 10 ns and τ_T = 2 ms. From the rate equations, it can be checked that the overall quantum yield values will not change significantly if lifetimes values around these ones are taken. We considered that these results corroborate the usefulness of the present model.

In the case of **1Tb**, $W_{\mathrm{CT}} = 0$ in Eqs. (S11) and (S14), due to the absence of the LMCT state. As discussed before, the LMCT state has a very short lifetime and is far apart from T_1 and Eu^{3+} acceptor levels. Therefore, we have not considered energy transfer from the LMCT to any other state. Another important point is the extremely resonance condition between S_1 and $^7F_5 \rightarrow {}^5F_5$($\Delta$=114 cm^{-1}) and $^7F_6 \rightarrow {}^5H_6$($\Delta$=109 cm^{-1}) states (pathways 10 and 3 in Table S8, respectively). This enables a high backward energy transfer rate $W_{\mathrm{bET}}^{\mathrm{S}}$in the same order of magnitude (1.04×10^7 and 0.50×10^7 s^{-1}, respectively) of the forward IET rate. If this is not considered, the value of the theoretical $Q_{\mathrm{Ln}}^{\mathrm{L}}$ grows to 67.6%, not agreeing so well with the experimental one.

As discussed before, the role of $^7F_5$ as an acceptor is crucial to describe the theoretical $Q_{\mathrm{Ln}}^{\mathrm{L}}$ of the **1Tb**. Otherwise, without its participation, the total W_{T} would decrease five orders of magnitude resulting in a $Q_{\mathrm{Ln}}^{\mathrm{L}}$ of 1.5%.

4 Conclusions

Based on the detailed crystallographic and spectroscopic analysis and theoretical calculations, it was demonstrated how a minor modification in the structure of Ln coordination compounds can result in major changes in their photophysical properties. The analysis was carried out on the example of Ln (**1Ln** and **2Ln**) coordination compounds with dimethyl(4-methylphenylsulfonyl)amidophosphate, crystallizing in the $P2_1/c$ (**1Ln**) and $C2/c$ (**2Ln**) space groups of the monoclinic system. The compounds share an identical first coordination sphere, while they differ in terms of presence of solvent molecules in the second coordination sphere (**1Ln-** does not contain solvent molecules, **2Ln** - contains solvent molecules).

Using the theoretical calculations of the nonradiative transition rates, the varying effect of shortening the Ln–O bonds (where O is the oxygen atom in the sulfonyl group) leading to either the increase (**1Tb**) or the decrease (**1Eu**) of the overall emission quantum yield was explained. The participation of the LMCT state in the depopulation of the ligand singlet state in the case of **1Eu** and the crucial role of the $^7F_5$ level in the energy transfer process in **1Tb** were demonstrated. Various energy transfer pathways were analyzed and it has been shown that the main pathways for sensitization of lanthanide emission are the triplet (**1Eu**) and singlet (**1Tb**) transfer, which in these cases occur mainly through the exchange mechanism.

It was shown and explained that a slight structural change in **1Ln** causes a blue shift of its excitation band in relation to the band observed for **2Ln**, while the maxima of the corresponding bands in absorption spectra remain unchanged. Furthermore, it was proved that additional splitting of the $^7F_1$ level of **1Eu** was a result of the resonance effect.

The analysis of properties of **1Ln** and **2Ln** and their subsequent comparison led to the conclusion that in addition to the proper chromophore selection, luminescent properties of the compounds in question can be noticeably modified through minor structural changes. Furthermore, it also showed that Ln coordination compounds in which the singlet transfer dominates may be characterized by high overall emission quantum yield. In addition, analyzing the properties of **1Eu** allowed to demonstrate some restrictions on the use of Eu^{3+} as a structural probe, for compounds in which the Eu^{3+} ion is well isolated by ligand molecules as well as the ones in which the Eu–Eu type energy transfer is absent.

Acknowledgments

The authors wish to acknowledge support through the grant of Minister of Science and Higher Education POIG.01.01.02–02–006/09 and the grant Minister of Science and Higher Education for young scientists 2432/M/WCH/14. This work was partially developed within the scope of the project CICECO-Aveiro Institute of Materials, FCT (Portuguese agency) Ref. UID/CTM/50011/2019, financed by national funds through the FCT/MCTES. A.N.C.N. also thanks SusPhotoSolutions–Soluções Fotovoltaicas Sustentáveis, CENTRO-01-0145-FEDER-000005.

Table 1. Continous Shape Measures (CShMs) of the coordination geometry for the Ln^{3+} ions in **1Eu**, **1Tb**, **2Eu** and **2Tb** [50]**.**

label	polyhedron's name	point group	CShM, Ln =			
			1Eu	**1Tb**	**2Eu**	**2Tb**
CU-8	cube	O_h	8.471	8.539	8.072	7.835
SAPR-8	square antiprism	D_{4d}	0.738	0.648	2.290	2.144
TDD-8	triangular dodecahedron	D_{2d}	1.139	1.247	0.183	0.252
JGBF-8	johnson – gyrobifastigium (J26)	D_{2d}	15.503	15.604	14.498	14.654
JETBPY-8	johnson - elongated triangular bipyramid (J14)	D_{3h}	28.759	28.688	29.773	29.495
JBTP-8	johnson - biaugmented trigonal prism (J50)	C_{2v}	2.222	2.211	2.681	2.629
BTPR-8	biaugmented trigonal prism	C_{2v}	1.863	1.919	2.468	2.459
JSD-8	snub disphenoid (J84)	D_{2d}	4.119	4.212	2.196	2.246
TT-8	triakis tetrahedron	T_d	9.333	9.389	8.456	8.139
HBPY-8	hexagonal bipyramid	D_{6h}	15.492	15.804	15.731	15.474

Table 2. The location and frequencies of the vibrational components related to vibrations in the IR spectrum a) in the range of emission spectrum, b) in the range of excitation spectrum.

a)

Number	**Lines (cm^{-1})**	**Frequencies (cm^{-1})**	**Maxima in IR spectra (cm^{-1})**
Relative to $^5D_0 \rightarrow {}^7F_0$			
ν_1	17 087	176	[a]
ν_2	17 075	187	186
ν_3	17 050	213	217
ν_4	17 036	227	220
ν_5	16 664	599	595.5
ν_6	16 511	752	750
ν_7	16 444	819	814
ν_8	16 397	866	864
Relative to $^5D_0 \rightarrow {}^7F_2(0,1,2)$			
ν_9	16 179	166 (0)	169

ν_{11}	16 131	159 (0)	155
ν_{12}	16 119	171 (1)	169
ν_{13}	16 108	182 (1)	186
ν_{14}	16 085	149 (2)	152
ν_{15}	16 062	172 (2)	169
ν_{16}	16 022	323 (0)	323
ν_{17}	15 962	328 (1)	323
ν_{18}	15 901	444 (0)	443
ν_{19}	15 795	550 (0)	550
ν_{20}	15 745	599 (0)	595.5
ν_{21}	15 540	750 (1)	750
ν_{22}	15 481	864 (0)	864

[a] in the range from 195 to 135 cm^{-1}broadband with maxima 186, 169, 155, 152 cm^{-1}

b)

Number	Lines (cm^{-1})	Frequencies (cm^{-1})	Maxima in IR spectra (cm^{-1})
	Relative to $^5D_0 \leftarrow {}^7F_0$		
ν_1	17 382	98	99.5
ν_2	17 477	193	186
ν_3	17 495	211	217
ν_4	18 147	863	864
ν_5	18 455	1171	1176
ν_6	18 750	1466	1462
ν_7	18 786	1502	1498
	Relative to $^5D_2 \leftarrow {}^7F_0$		
ν_7'	21 714	160	155
ν_8'	21 772	218	213
ν_9'	21 857	296	296.5
ν_{10}'	21 875	321	323
ν_{11}'	21 898	344	341.5
ν_{12}	22 009	455	450
ν_{13}	22 153	599	595.5
ν_{14}	22 418	864	864
ν_{15}	22 617	1063	1058
ν_{16}	22 651	1097	1082
ν_{17}	22 707	1153	1158
ν_{18}	22 741	1187	1191
ν_{19}	24 398	2844	2851.5
ν_{20}	24 440	2870	2866
ν_{21}	24 468	2951	2955

Table 3. Selected photophysical data of **1Ln** and **2Ln**.

compound	τ(ms)		Q_{Ln}^{Ln} (%)	Q_{Ln}^{L} (%)	η (%)
	293 K	77 K			

1Eu	2.30	2.30	77	3.6[a]	4.7
2Eu[8]	2.51	2.50	74	16.6	22
1Tb	2.41	2.50		58[a]	
2Tb[8]	2.78	2.79	79	36	47

Estimated error of 10% on the quantum yields Q_{Ln}^{Ln} and Q_{Ln}^{L}; [a]λ_{exc} = 275 nm.

Table 4. Experimental and theoretical Q_{Ln}^{L} for **1Eu** and **1Tb**.

Coordination compounds	**1Eu**	**1Tb**
Q_{Ln}^{L} (experimental)	3.6%	58%
Q_{Ln}^{L} (theoretical)	3.6%	57%

Figure Captions:

Figure 1. Structural formulae of the ligands **HL.**

Figure 2. The X-ray crystal structure of **1Eu**: view of crystal packing along the *c* axis (A), molecular structure of 1Eu (H atoms are omitted for clarity and the disorder of —OCH_3 groups is marked in a transparent manner) (B), coordination polyhedron of the Eu ion (C).

Figure 3.FTIR spectra of **1Tb** and **2Eu,** * denotes frequencies visible as vibrational components in emission and excitation spectra.

Figure 4. The diffuse reflectancespectraof **1Eu** and **1Gd** at 293 K.

Figure 5. The phosphorescent spectra of **1Na** (λ_{exc} = 270 nm, orange line), **1La** (blue line) and **1Gd** (grey line) at λ_{exc} = 280 nm at 77 K and 293 K (black line).

Figure 6. The excitation spectra of **1Gd** (λ_{mon}= 430 nm) phosphorescence monitoring at 77K and **1La** (λ_{mon}= 305 nm) at 293 K – fluorescence monitoring.

Figure 7. The emission bands of **1Eu** and **2Eu** (λ_{exc} = =394.5 nm) corresponding to the transitions: $^5D_0 \rightarrow {}^7F_1$ (top, (A)), $^5D_0 \rightarrow {}^7F_{0,2}$ (middle (B)), $^5D_0 \rightarrow {}^7F_4$ (bottom (C)) at 77K.

Figure 8. The excitation spectra of **1Tb** at 293 and 77 K, λ_{mon} = 542.6 nm.

Figure 9. The excitation spectra of **1Eu** at 293 and 77 K, λ_{mon} = 613.0 nm.

Figure10. The excitation spectra of **1Eu, 2Eu, 1Tb** and **2Tb** at 293 K.

Figure 11. Molecular orbitals compositions for the formation of excited T_1 (left panel) and S_1(right panel) states. In both cases, the final molecular orbitals (the unoccupied ones; the ligand donor states) are located at the aromatic ring.

Figure 12. Energy level diagrams for **1Eu** (left panel) and **1Tb** (right panel). ϕ is the pumping rate. τ_S, τ_T, τ_{CT}, and τ_4 are the lifetimes of the S_1, T_1, LMCT, and emitting states, respectively. In order to facilitate the setup of the *rate equations* (Supporting Information), groups of levels have been represented in brackets $|n\rangle$. However, and most importantly, is that each energy transfer rate pathway has been calculated individually as shown in Tables S7 and S8.

References

1. Bünzli JCG. Lanthanide light for biology and medical diagnosis. *J Lumin.* 2016;170(Part 3):866.
2. Butler SJ, Delbianco M, Lamarque L,McMahon BK,Neil ER, Pal R et al. EuroTracker® dyes: Design, synthesis, structure and photophysical properties of very bright europium complexes and their use in bioassays and cellular optical imaging. *Dalt Trans.* 2015;44(11):4791.
3. Bui AT, Roux A, Grichine A, Duperray A, Andraud C, Maury O. Twisted Charge-Transfer Antennae for Ultra-Bright Terbium(III) and Dysprosium(III) Bioprobes. ChemEurJ. 2018;24(14):3408.
4. Aslandukov AN, Utochnikova V V, Goriachiy DO, Vashchenko AA, Tsymbarenko DM, Hoffmann M, et al. The development of a new approach toward lanthanide-based OLED fabrication: new host materials for Tb-based emitters. *Dalt Trans.* 2018;47(45):16350.
5. Fix T, Nonat A, Imbert D, Pietro SD,Mazzanti M,Slaoui A, et al. Enhancement of silicon solar cells by downshifting with Eu and Tb coordination complexes. *ProgPhotovolt Res Appl.* 2016;24(6):12515.
6. Bünzli JCG, Eliseeva S V. Lanthanide NIR luminescence for telecommunications, bioanalyses and solar energy conversion. *J Rare Earths.* 2010;28(6):824.
7. Sabbatini N, Guardigli M, Lehn JM. Luminescent lanthanide complexes as photochemical supramolecular devices. *Coord Chem Rev.* 1993;123(1–2):201.
8. Kasprzycka E, Trush VA, Amirkhanov VM, Jerzykiewicz L, Malta OL, Legendziewicz J et al. Contribution of energy transfer from the singlet state to the sensitization of Eu^{3+} and Tb^{3+} luminescence by sulfonylamidophosphates. *Chem Eur J.* 2017;23(6):1318.
9. Olyshevets I, Kariaka N, Znovjyak K, Gerasimchuk N, Lindeman S, Smola S et al. Synthesis and characterization of anionic lanthanide(III) complexes with a bidentate sulfonylamidophosphate (SAPh) ligand. *Inorg Chem.* 2020;59(1):76.
10. Sobczyk M, Korzeniowski K, Guzik M, Cybińska J,Gerasymchuk Y, Trush VA et al. Spectroscopic behaviour of $Na[Sm(SP)_4]$ (where $SP = C_6H_5S(O)_2NP(O)(OCH_3)_2^-$) and its polymeric material-new orange emitting phosphors. *J Lumin.* 2018;193:90.
11. Kasprzycka E, Trush VA, Jerzykiewicz L, Amirkhanov VM, Watras A,Sokolnicki J et al. Lanthanide complexes with phosphorylated 2-naphthylsulfonamides ligands as electromagnetic radiation converters. *Dye Pigment.* 2019;160:439.
12. Prytula-Kurkunova AY, Pichon C, Duhayon C, Amirkhanov VM, Sutter JP. Mononuclear lanthanide complexes containing [O–O]-chelating sulfonylamidophosphate type ligands. *Eur J Inorg Chem*. 2019;3:4592.
13. Marek Ł, Sobczyk M, Trush VA, Korzeniowski K, Amirkhanov VM, Legendziewicz J. Synthesis, structure and radiative and nonradiative properties of a new Dy^{3+} complex with sulfonylamidophosphate ligand. *J Rare Earths.* 2019;37(11):1255.
14. Amirkhanov V, Ovchynnikov VA, Trush VA, Gawryszewska P, Jerzykiewicz LB. Powerful new ligand systems: carbacylamidophosphates (CAPH) and sulfonylamidophosphates (SAPH). In: Gawryszewska P, Smoleński P, eds. *Ligands. Synthesis, Characterization and Role in Biotechnology.* New York: NOVA publishers; 2014:199.
15. Kasprzycka E, Trush VA, Jerzykiewicz L, Amirkhanov VM, Gawryszewska P. Structural and spectroscopic properties of Nd complexes with sulfonylamidophosphate type ligands. *J Lumin*. 2015;170(Part 2):3487.
16. CrysAlisPRO Software system, Version 1.171.38.41 (2015). Rigaku Oxford Diffraction, Rigaku Corporation, Oxford, U.K.
17. SHELXL, Sheldrick GM. **Crystal structure refinement**. ***ActaCryst.* 2015; C71:3–8.**

18. Brandenburg K, Putz H. Diamond: Crystal and Molecular Structure Visualization. Cryst Impact Bonn, Germany 2008.http://www.crystalimpact.com/diamond.
19. Frisch MJ, Trucks GW, Schlegel HB, Scuseria GE, Robb MA, Cheeseman JR, et al. Gaussian 09, Revision D.01, (2013).

20. Chai JD, Head-Gordon M. Long-range corrected hybrid density functionals with damped atom-atom dispersion corrections. *Phys ChemChem Phys*. 2008;10(44):6615.
21. Dunning TH. Gaussian basis sets for use in correlated molecular calculations. I. The atoms boron through neon and hydrogen. *J Chem Phys.* 1989;90(2):1007.
22. Pipek J, Mezey PG. A fast intrinsic localization procedure applicable for ab initio and semiempirical linear combination of atomic orbital wave functions. *J Chem Phys*. 1989;90(9):4916.
23. Schmidt MW, Baldridge KK, Boatz JA, Elbert ST, Gordon MS, Jensen JH et al. General atomic and molecular electronic structure system. *J Comput Chem.* 1993;14(11):1347.
24. teVelde G, Bickelhaupt FM, Baerends EJ, Guerra CF,van Gisbergen SJA, Snijders JG et al. Chemistry with ADF. *J Comput Chem*. 2001;22(9):931.

25. Becke AD. Density-functional exchange-energy approximation with correct asymptotic behavior. *Phys Rev A*. 1988;38(6):3098.
26. Perdew JP. Density-functional approximation for the correlation energy of the inhomogeneous electron gas. *Phys Rev B.* 1986;33(12):8822.
27. Van Lenthe E, Baerends EJ. Optimized Slater-type basis sets for the elements 1–118. *J Comput Chem.* 2003;24(9):1142.
28. Van Lenthe E, Snijders JG, Baerends EJ. The zero-order regular approximation for relativistic effects: The effect of spin-orbit coupling in closed shell molecules. *J Chem Phys*. 1996;105(15):6505
29. Van Lenthe E, Baerends EJ, Snijders JG. Relativistic total energy using regular approximations. *J Chem Phys.* 1994;101(11):9783.
30. Van Lenthe E. Geometry optimizations in the zero order regular approximation for relativistic effects. *J Chem Phys*. 1999;110(18):8943.
31. Malta OL. Ligand—rare-earth ion energy transfer in coordination compounds. A theoretical approach. *J Lumin*. 1997;71(3):229.
32. Malta OL, Gonçalves e Silva FR. A theoretical approach to intramolecular energy transfer and emission quantum yields in coordination compounds of rare earth ions. *SpectrochimActa Part A MolBiomolSpectrosc*. 1998;54(11):1593–1599. doi:10.1016/S1386–1425(98)00086–9.
33. Longo R, Gonc FR. A theoretical study of the energy-transfer process in $[Eu\subset bpy.bpy.bpy]^{3+}$cryptates: a ligand-to-metal charge-transfer state? *Chem Phys Lett*. 2000;328(1–2):67.
34. Malta OL. Mechanisms of non-radiative energy transfer involving lanthanide ions revisited. *J Non Cryst Solids*. 2008;354(42–44):4770.
35. Judd BR. Optical absorption intensities of rare-earth ions. *Phys Rev*. 1962;127(3):750.
36. Ofelt GS. Intensities of Crystal Spectra of Rare□Earth Ions. *J Chem Phys*. 1962;37(3):511.
37. Malta OL. Theoretical crystal-field parameters for the YOCl:Eu^{3+}system. A simple overlap model. *Chem Phys Lett*. 1982;88(3):353.
38. Malta OL. A simple overlap model in lanthanide crystal-field theory. *Chem Phys Lett*. 1982;87(1):27.
39. Carnall WT, Crosswhite H, Crosswhite HM. *Energy Level Structure and Transition Probabilities in the Spectra of the Trivalent Lanthanides in LaF3*. United States. 1978.doi:10.2172/6417825
40. Carneiro Neto AN, Teotonio EES, de Sá GF, Brito HF, Legendziewicz J, Carlos LD,et al. Modeling intramolecular energy transfer in lanthanide chelates : a critical review and recent advances, In: *Handb. Phys. Chem. Rare Earths Vol 56*, Elsevier, 2019:55.
41. Ofelt GS. Structure of the f^6 configuration with application to rare-earth ions. *J Chem Phys*. 1963;38(9):2171.
42. Malta OL, Brito HF, Menezes JFS, Gonçalves e Silva FR, Alves Jr S, Farias Jr FS et al. Spectroscopic properties of a new light-converting device Eu(thenoyltrifluoroacetonate)$_3$ 2(dibenzyl sulfoxide). A theoretical analysis based on structural data obtained from a sparkle model. *J Lumin*. 1997;75(3):255.
43. Souza AS, Nunes LA, Felinto MCFC, Brito HF, Malta OL. On the quenching of trivalent terbium luminescence by ligand low lying triplet state energy and the role of the $^7F_5$ level: The $[Tb(tta)_3(H_2O)_2]$

case. *J Lumin*. 2015;167:167.
44. Roy UN, Hawrami RH, Cui Y, Morgan S, Burger A. Tb^{3+}-doped KPb_2Br_5: Low-energy phonon mid-infrared laser crystal. *Appl Phys Lett*. 2005;86(15):151911.
45. Rademaker K, Krupke WF, Page RH, Payne SA, Petermann K,Huber G, et al. Optical properties of Nd^{3+}- and Tb^{3+}-doped KPb_2Br_5 and $RbPb_2Br_5$ with low nonradiative decay. *J Opt Soc Am B*. 2004;21(12):2117..
46. Faustino WM, Malta OL, De Sá GF. Intramolecular energy transfer through charge transfer state in lanthanide compounds: A theoretical approach. *J Chem Phys*. 2005;122(5).
47. Kulesza D, Sobczyk M, Legendziewicz J, Moroz OM, Amirkhanov VM. Structure and spectroscopy of NaNd(SP)4 chelate: A new type of lanthanide luminophore. *Struct Chem*. 2010;21(2):425.
48. Shatrava IO, Sliva TY, Ovchynnikov VA, Konovalova IS, Amirkhanov V. catena-Poly[neodymium(III)-bis[l-N- (dimorpholinophosphoryl)benzene-sulfonamidato]-sodium(I)-bis[l-N-(dimorpholinophosphoryl) benzene- sulfonamidato]]. *ActaCrystallogr Sect E*. 2010;E66:m397-.
49. Kishino S, Saito S, Kudamatsu A, Shiokawa K, Tsuboi S. O-Alkyl-S-n-propyl-N-sulfonyl-phosphoric acid ester amides. United States Patent, US4161524A,1979.
50. Llunell M, Casanova D, Girera J,Alemany P, Alvarez S, SHAPE, version 2.0, Barcelona, Spain, 2010.
51. Binnemans K, Görller-Walrand C. Application of Eu^{3+} ion for site symmetry determination. *J Rare Earths*. 1996;14:173.
52. Malta O. The theory of vibronic transitions in rare earth compounds. *J Phys Chem Solids*. 1995;56(8):1053
53. Berry MT, Kirby AF, Richardson FS. Vibronic transitions in the excitation and emission spectra of hexakis(Antipyrine)europium(III) tri-iodide and tri-perchlorate crystals. *Mol Phys*. 1989;66(4):723.
54. Gałdecka E, Gałdecki Z, Huskowska E, Amirkhanov VM, Legendziewicz J. Crystal structure and optical properties of Ln(III) octahedral complexes with hexamethylphosphortriamide; $[Ln(HMPA)_6](ClO_4)_3$. *J Alloys Compd*. 1997;257:182.
55. Tsaryuk V, Zolin V, Legendziewicz J. Vibronic spectra of europium compounds containing derivatives of 1,10-phenanthroline. *SpectrochimActa - Part A MolBiomolSpectrosc*. 1998;54(13):2247.
56. Caro P, Moune OK, Antic-Fidancev E, Lemaitre-Blaise M. Vibronic optical transitions in inorganic and organic rare earth materials. *J Less-Common Met*. 1985;112(1–2):153.
57. Gerlinger H, Schaack G. Crystal-field states of the Ce^{3+} ion in CeF_3: A demonstration of vibronic interaction in ionic rare-earth compounds. *Phys Rev B*. 1986;33(11):7438.
58. Blasse G, Dirksen GJ, Sabbatini N, Perathoner S, Lehn JM, Alpha B. Luminescence processes in $[Tb{\subset}bpy{\cdot}bpy{\cdot}bpy]^{3+}$cryptate: A low-temperature solid-state study. *J Phys Chem*. 1988;92(9):2419
59. Gawryszewska P, Ciunik Z. Structure and photophysical properties of new lanthanide(III) complexes $[Ln(_{C10H8O6)1.5}(H2O)_3]_{H2}O$. *J PhotochemPhotobiol A Chem*. 2009;202(1):1
60. Faustino WM, Malta OL, de Sá GF. Theoretical modeling of thermally activated luminescence quenching through charge transfer states in lanthanide complexes. *Chem Phys Lett*. 2006;429(4–6):595

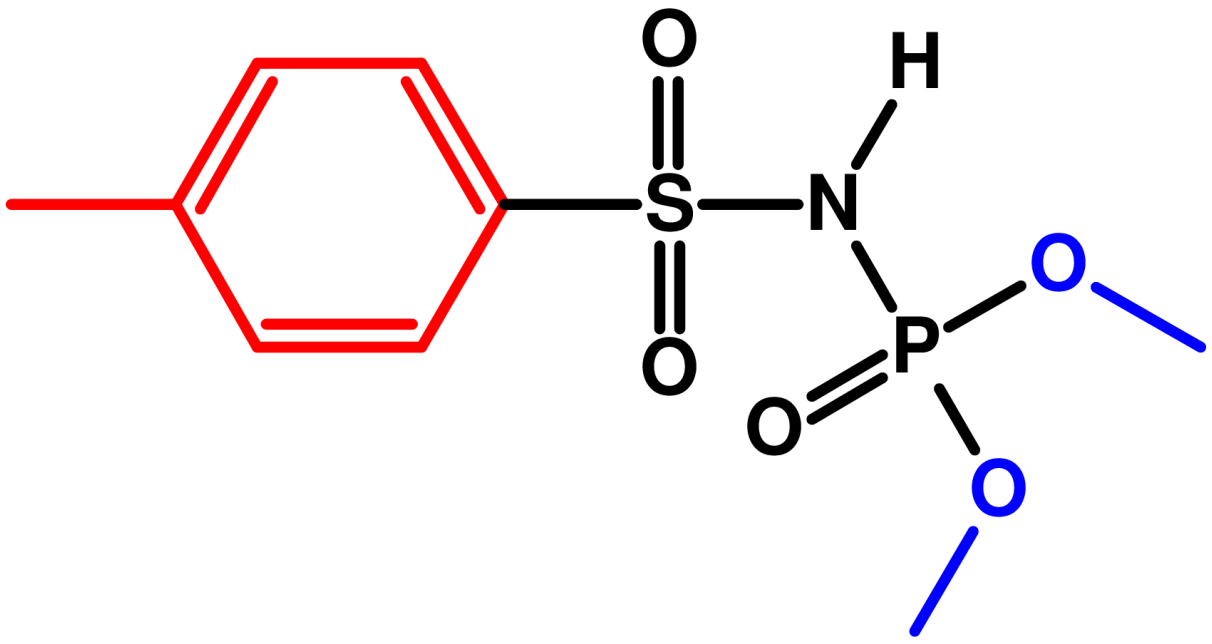

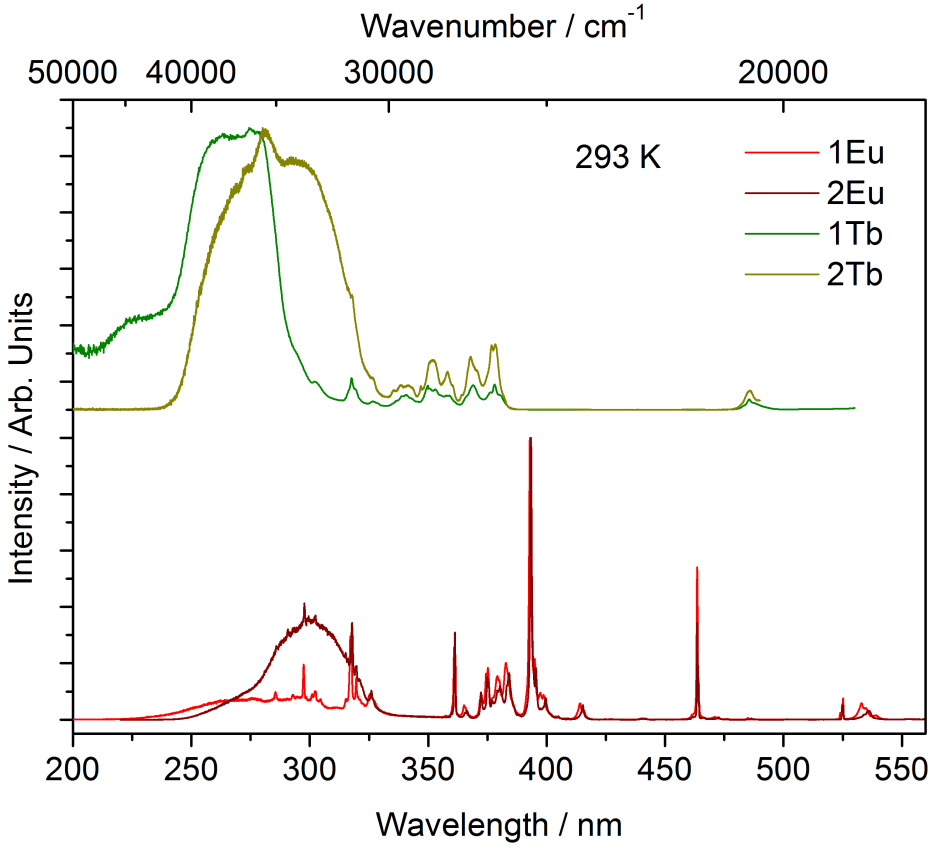
Wavenumber / cm-1
50000
40000
30000
20000
293 K
1Eu
2Eu
1Tb
2Tb
Intensity / Arb. Units
200
250
300
350
400
450
500
550
Wavelength / nm

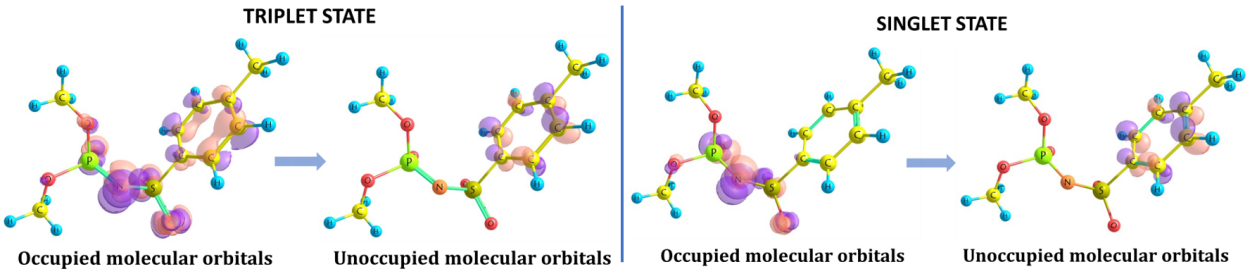

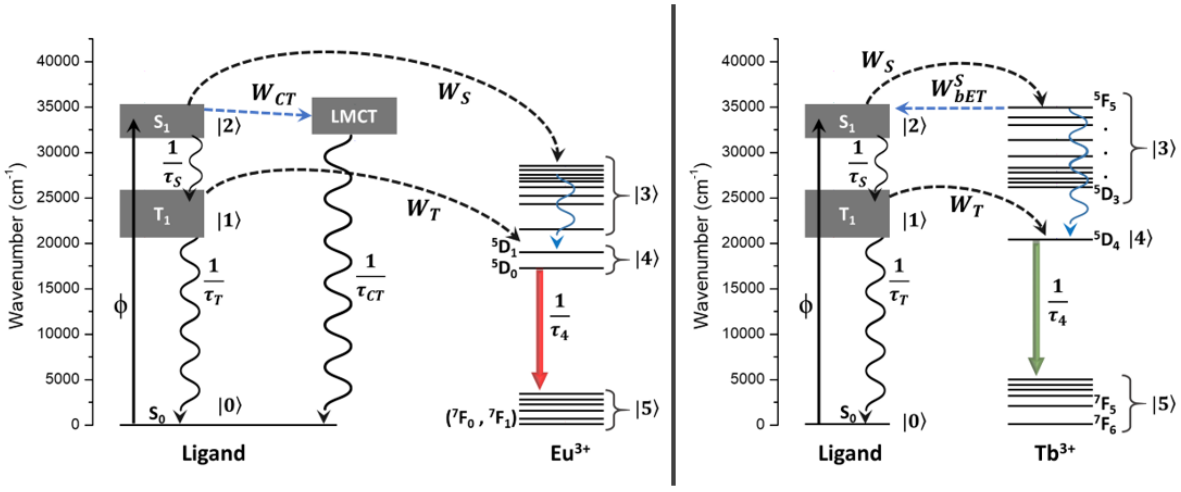

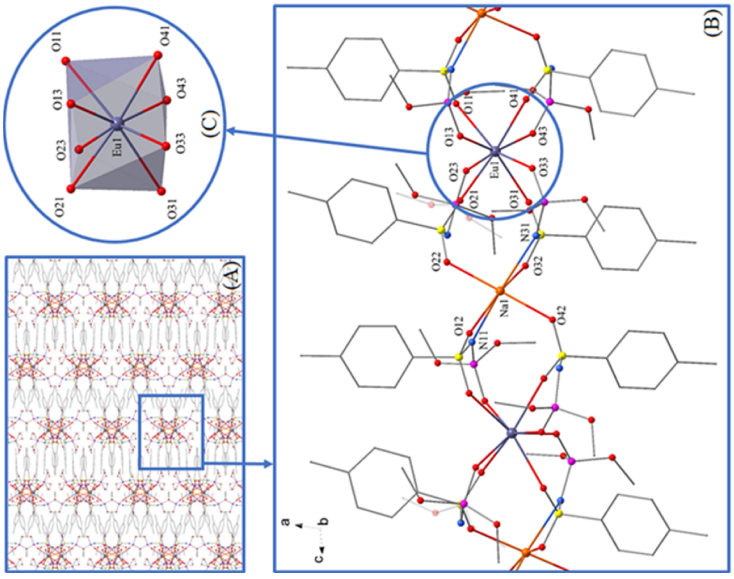
(A)
(B)
(C)
O11
O41
O13
O43
O23
Eu1
O33
O21
O31
O22
O32
Na1
O12
N11
O42
N31
a
b
c

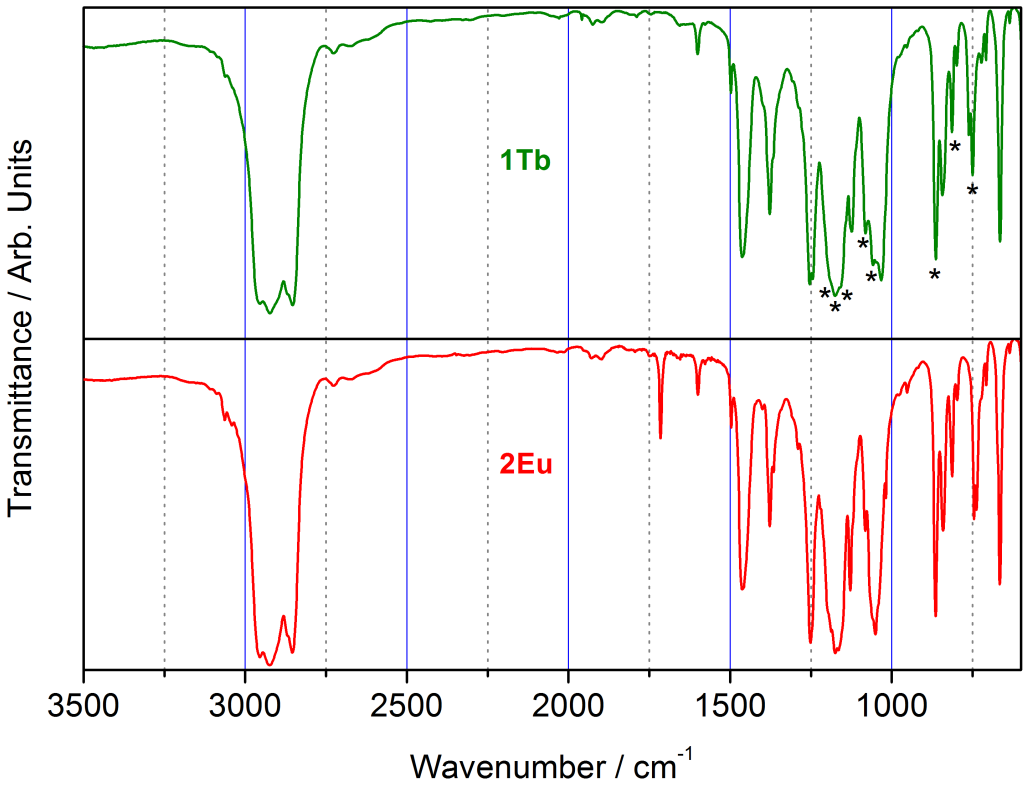
Transmittance / Arb. Units
1Tb
2Eu
3500
3000
2500
2000
1500
1000
Wavenumber / cm-1

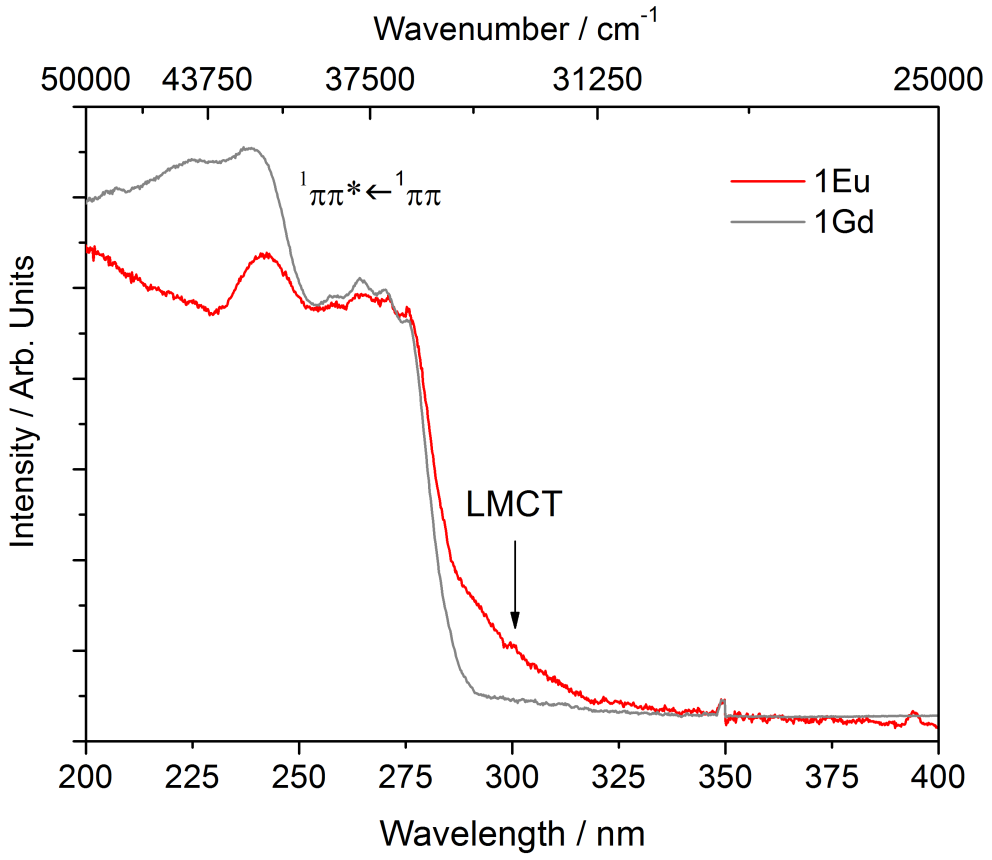
Wavenumber / cm-1
50000
43750
37500
31250
25000
Intensity / Arb. Units
1ππ*←1ππ
1Eu
1Gd
LMCT
200
225
250
275
300
325
350
375
400
Wavelength / nm

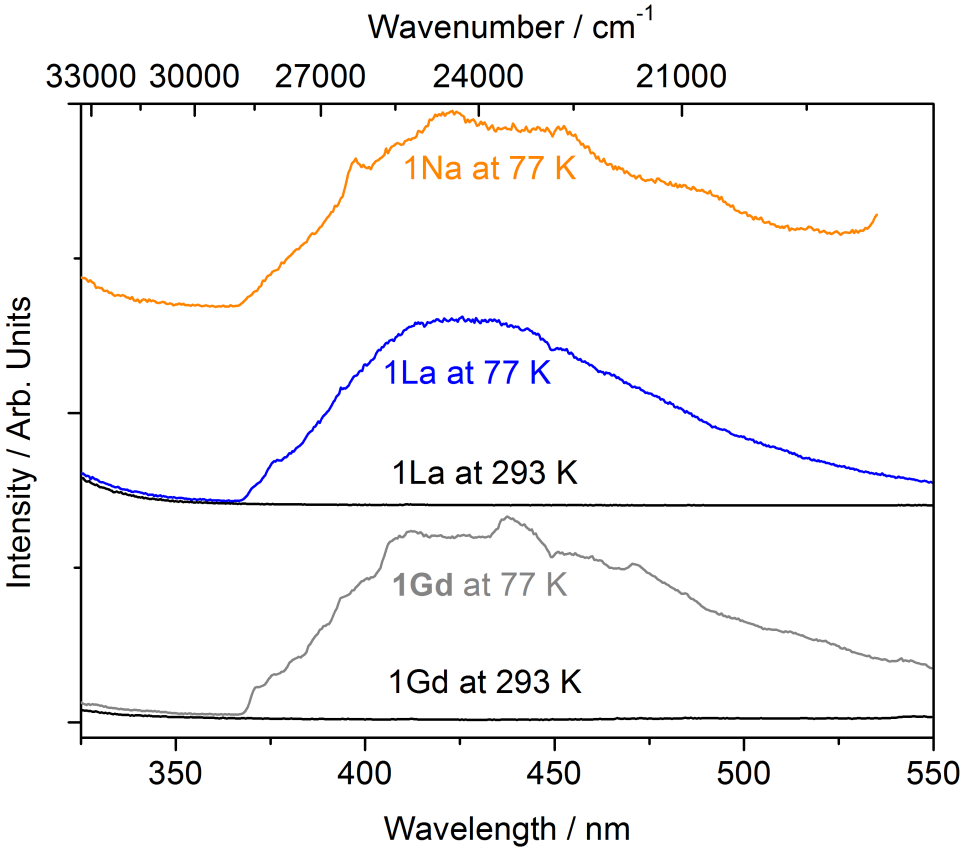
Wavenumber / cm-1
33000 30000 27000 24000 21000
1Na at 77 K
1La at 77 K
1La at 293 K
1Gd at 77 K
1Gd at 293 K
Intensity / Arb. Units
350 400 450 500 550
Wavelength / nm

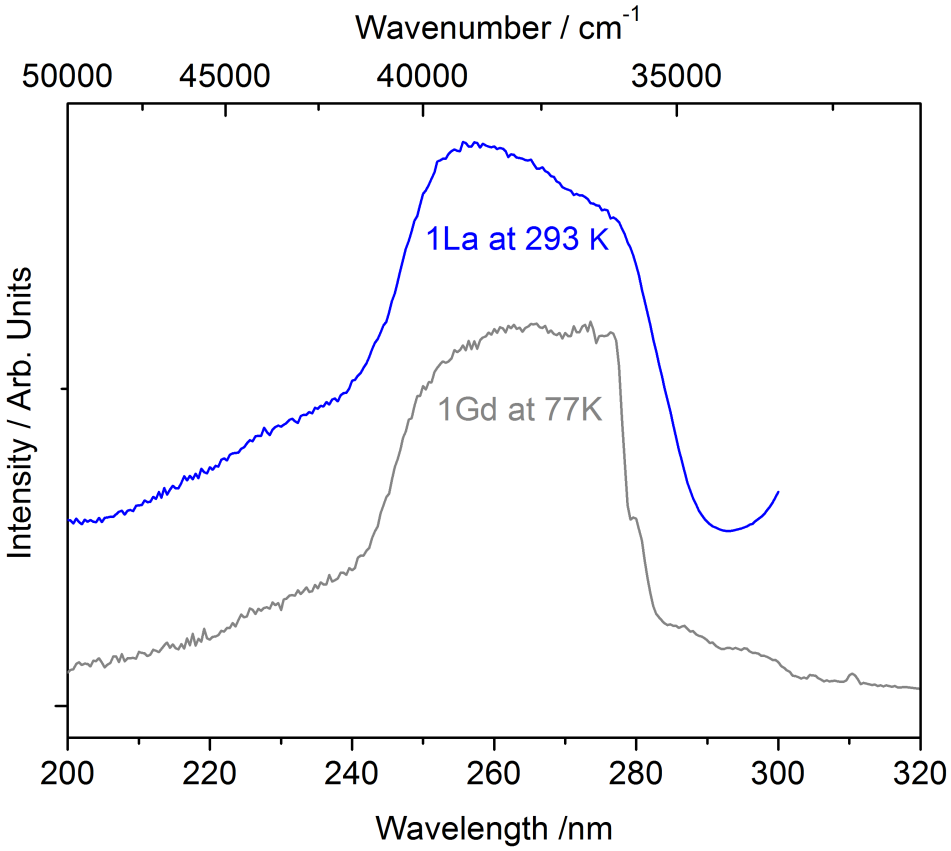
Wavenumber / cm-1
50000
45000
40000
35000
1La at 293 K
1Gd at 77K
Intensity / Arb. Units
200
220
240
260
280
300
320
Wavelength /nm

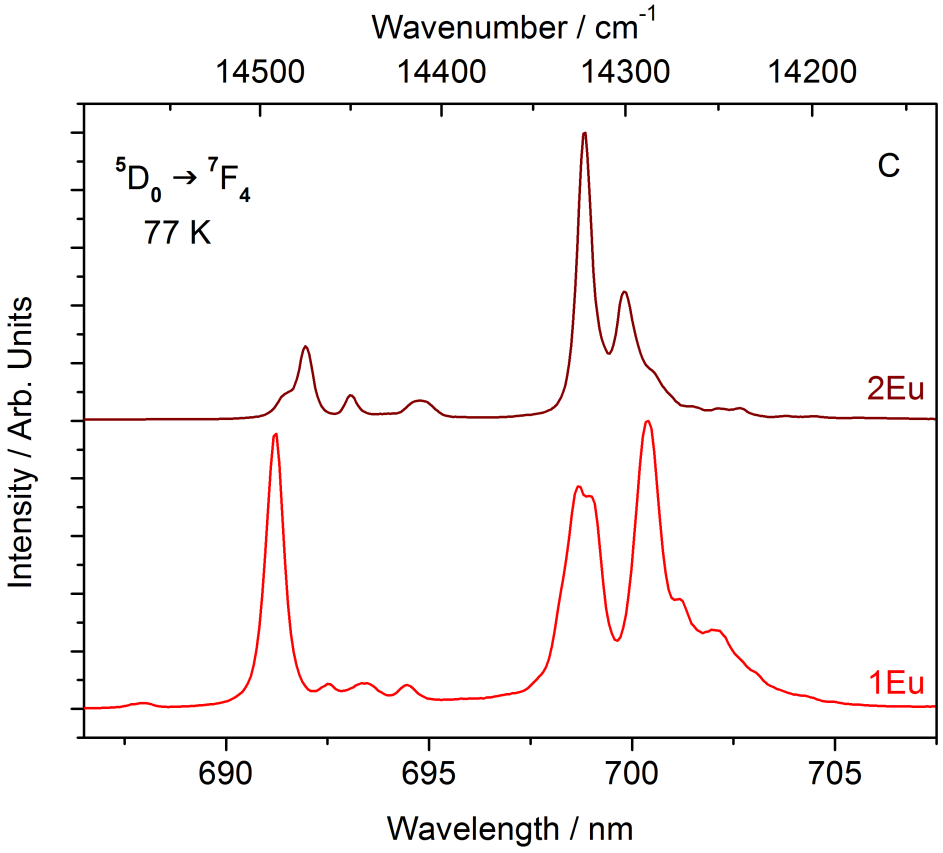
Wavenumber / cm-1
14500
14400
14300
14200
5D0 → 7F4
77 K
C
2Eu
1Eu
Intensity / Arb. Units
690
695
700
705
Wavelength / nm

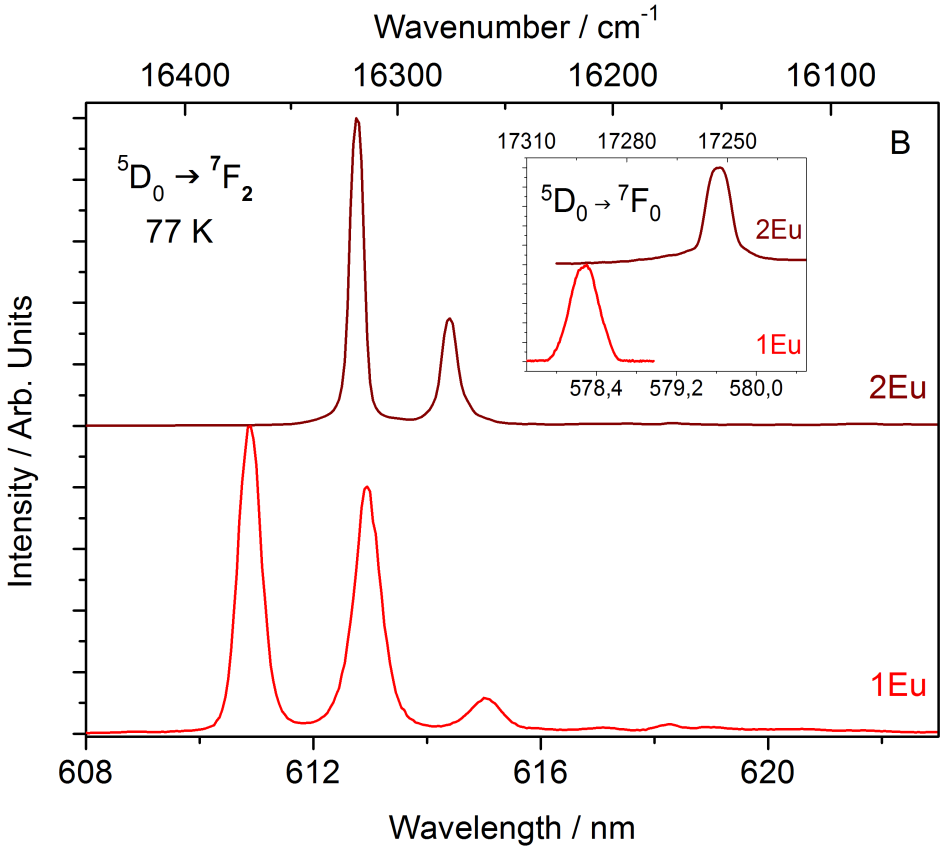
Wavenumber / cm-1
16400
16300
16200
16100
5D0 → 7F2
77 K
B
17310
17280
17250
5D0 → 7F0
2Eu
1Eu
578,4
579,2
580,0
2Eu
1Eu
Intensity / Arb. Units
608
612
616
620
Wavelength / nm

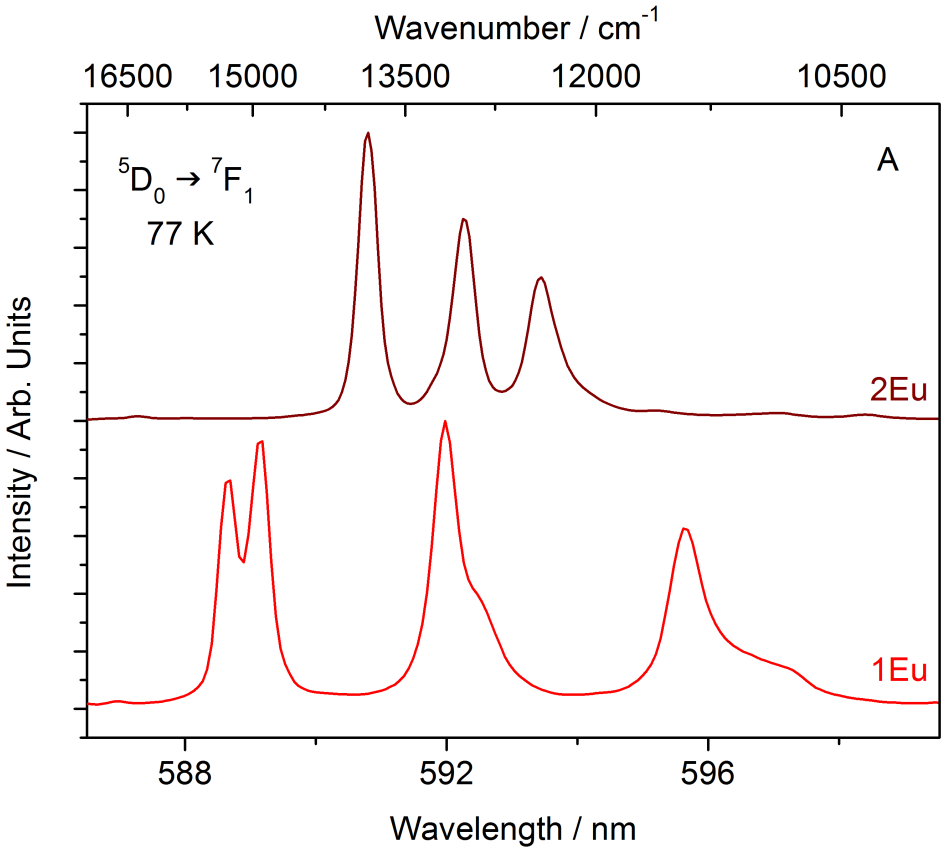
Wavenumber / cm-1
16500
15000
13500
12000
10500
5D0 → 7F1
77 K
A
2Eu
1Eu
Intensity / Arb. Units
588
592
596
Wavelength / nm

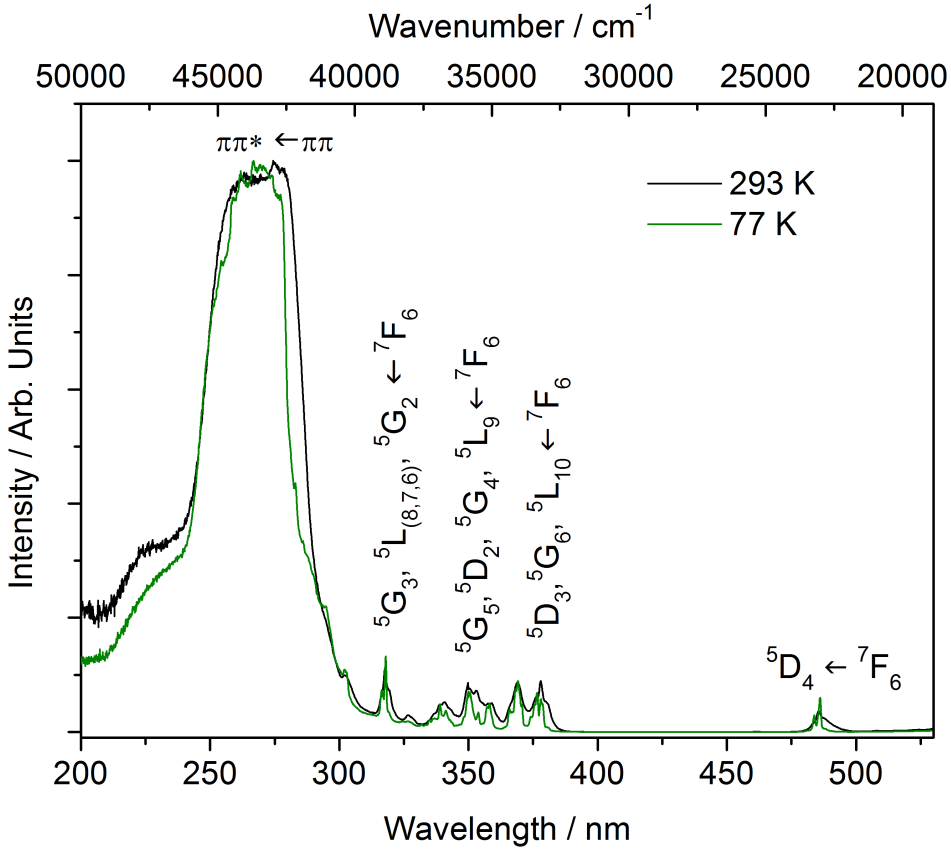
Wavenumber / cm-1
50000
45000
40000
35000
30000
25000
20000
ππ* ←ππ
293 K
77 K
Intensity / Arb. Units
5G3, 5L(8,7,6), 5G2 ← 7F6
5G5, 5D2, 5G4, 5L9 ← 7F6
5D3, 5G6, 5L10 ← 7F6
5D4 ← 7F6
200
250
300
350
400
450
500
Wavelength / nm

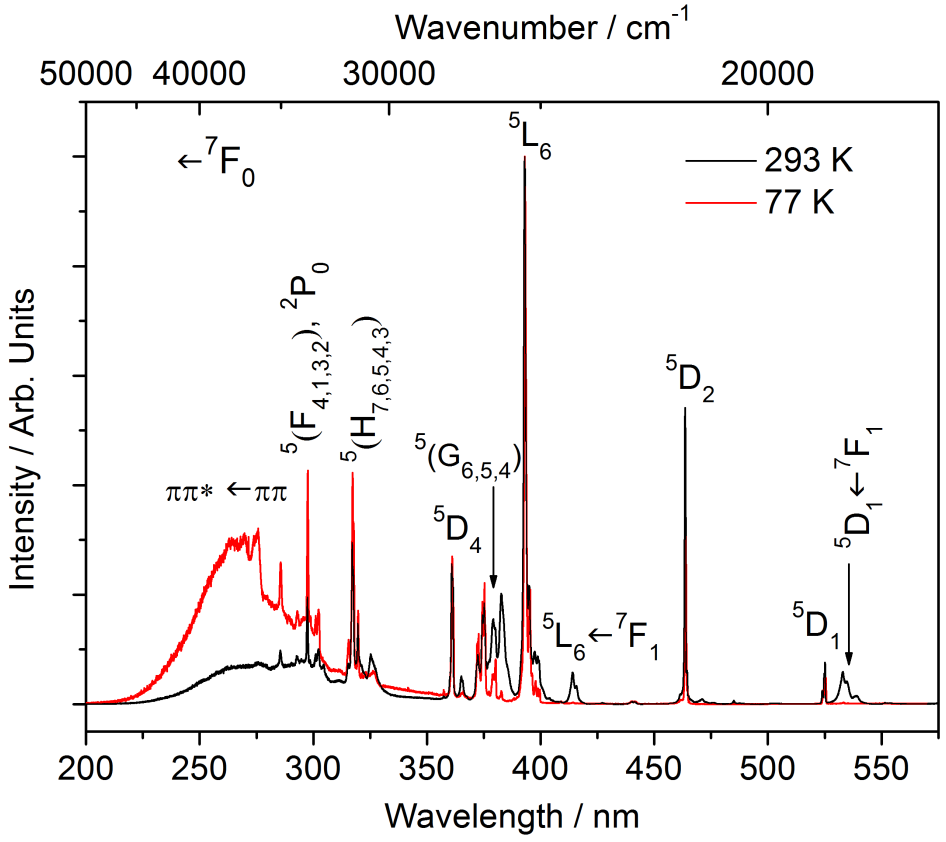
Wavenumber / cm-1
50000
40000
30000
20000
293 K
77 K
←7F0
5L6
5D2
5D1←7F1
5(F4,1,3,2), 2P0
5(H7,6,5,4,3)
5(G6,5,4)
5D4
ππ* ←ππ
5L6←7F1
5D1
Intensity / Arb. Units
200
250
300
350
400
450
500
550
Wavelength / nm

Highlights:

- Two series of the Ln complexes with the same first coordination sphere were obtained.
- It was shown how minor structural changes cause major consequences in their photophysical properties.
- The crucial role of the $^7F_5$ level and the LMCT state in the energy transfer process was demonstrated.
- The main pathways for sensitization of the lanthanide emission are the triplet (**1Eu**) and singlet (**1Tb**) transfer occurring mainly through the exchange mechanism.

Declaration of interests

☒ X The authors declare that they have no known competing financial interests or personal relationships that could have appeared to influence the work reported in this paper.

☐The authors declare the following financial interests/personal relationships which may be considered as potential competing interests: